Hybrid systems based on gas turbine combined cycle for trigeneration of power, cooling, and freshwater: A comparative techno-economic assessment

Kasra Mohammadi[1]*, Mohammad Saeed Efati Khaledi[2], Mohammad Saghafifar[3], Kody Powell[4]

[1, 4] University of Utah, Department of Chemical Engineering, 50 South Central Campus Dr., 3290 MEB, Salt Lake City, UT 84112-9203, USA

[2]Independent researcher, Tehran, Iran

[3] Department of Engineering, University of Cambridge, Trumpington Street, Cambridge CB2 1PZ, United Kingdom

*Corresponding author email address: kasra.mohammadi@utah.edu

ABSTRACT

The objective of this study is to develop and thoroughly evaluate several feasible hybrid trigeneration configurations based on a gas turbine combined cycle (GTCC) for generating electricity, freshwater, and cooling. Six hybrid configurations are developed by integrating different desalination and chiller systems to the GTCC. Desalination systems include multi effect distillation (MED) and reverse osmosis (RO) with pressure exchanger (PEX) and chiller systems include double effect and half effect water-lithium bromide absorption chillers (DEABC and HEABC) and a vapor compression chiller (VCC) with different working fluids. The specific goal is to identify the optimal hybridization scheme and parameters among different configurations. The economic results show that implementation of RO is more economical than a hybrid MED-RO system in which the power cycle's condenser is replaced by a MED. Also, the use of DEABC is more economical than a HEABC and a VCC. The results demonstrate that configuration 1 in which GTCC with the wet cooling tower is integrated with DEABC and RO is the most economical configuration. For this system, the levelized costs of electricity, water, and cooling (LCOE, LCOW, LCOC) are \$0.0648/kWh, \$0.7219/m^3 and \$0.0402/ton-hr, respectively, of which LCOE and LCOC are not the lowest values among different configurations.

Keywords: Hybrid trigeneration systems; Gas turbine combined cycle; Desalination systems; Water-Lithium bromide absorption chillers; Thermo-economic analysis.

Nomenclature

Acknowledgement: This material is based upon work supported by the U.S. Department of Energy's Office of Energy Efficiency and Renewable Energy (EERE) under the Advanced Manufacturing Office Award Number DE-EE0007712.

A	absorber	P	pressure (kPa)
ABC	absorption chiller	PR	pressure ratio
BPE	boiling point elevation	PEX	pressure exchanger
C	compressor	$\dot{Q}$	heat transfer rate (kW)
CC	combustion chamber	RO	reverse osmosis
Cond	condenser	SEABC	single effect absorption chiller
COP	coefficient of performance (−)	T	temperature (°C)
DEABC	double effect absorption chiller	TIT	turbine inlet temperature
Evap	evaporator	TTD	terminal temperature difference
EG	electrical generator	Turb	Turbine
FB	flash box	VCC	vapor compression chiller
Gen	generator	$\dot{W}$	work (kW)
GOR	gain output ratio	X	salinity of water (ppm)
GTCC	gas turbine combined cycle		
h	enthalpy (kJ/kg)	***Symbols***	
HP	high pressure	ϵ	effectiveness
HT	high temperature	λ	latent heat
HEABC	half effect absorption chiller	η	energy efficiency
HEX	heat exchanger		
LCOC	levelized cost of cooling ($/ton-hr)	***Subscripts***	
LCOE	levelized cost of electricity ($/kWh)	c	condensate
LCOW	levelized cost of water ($/m^3)	B	Brine
LiBr	lithium bromide	D	distillate
LP	low pressure	F	feed seawater
LT	low temperature	in	Input
$\dot{m}$	mass flow rate (kg/s)	$isen$	isentropic
MED	Multi-effect distillation	out	Outlet
NH_3	ammonia	S	Steam
N	number of effects	SW	sea water
OFWH	open feed water heater	wb	wet bulb

1. Introduction

Despite the substantial progress over the past few decades, the world is still experiencing significant challenges for supplying growing energy demand in a clean and sustainable manner in order to mitigate climate change. Along with electricity, demand for freshwater and air conditioning are on the rise in most parts of the globe. This is a strong motivation for continued research and development to create innovative solutions to meet these needs. Energy recovery is one of the most effective routes to improve the energy efficiency and sustainability of industrial processes and power generation cycles [1, 2]. This method is utilized in processes where unused thermal energy is accessible or available thermal energy can be extracted and used efficiently for other purposes.

Various means of heat utilization may be considered, depending on the amount and quality of the available heat. This leads to improved energy utilization efficiency by having industrial processes with a variety of products. One possibility is to use the available heat to operate thermally-driven cooling and refrigeration cycles. These processes can be categorized into absorption chillers using water-lithium bromide (H_2O-LiBr) or ammonia-water (NH_3-H_2O) as a working fluid, adsorption chillers, and solid and liquid desiccant systems [3]. The available heat can also be utilized to produce clean water via thermal desalination processes. The main types of thermal desalination technologies, that operate based on evaporation and condensation phenomena, are multi-effect distillation (MED), multi-stage flash distillation (MSF), thermal vapor compression (TVC), membrane distillation (MD), and humidification-dehumidification (HDH) systems [4].

Trigeneration and multigeneration systems provide an opportunity to supply a mix of different products simultaneously through recovering the available heat and improving energy utilization [5]. This leads to improved economic and environmental performance [6]. A large number of studies have been presented in the open literature to propose, model, and evaluate different trigeneration and multigeneration technologies and configurations. For example, Ahmadi et al. [7] evaluated a multigeneration system driven by waste heat from industry, for producing power, cooling, heating, and hydrogen. The system was comprised of an organic Rankine cycle (ORC), an ejector refrigeration cycle, a domestic water heat exchanger and an electrolyzer driven by the ORC. The authors utilized multi-objective optimization to identify the optimum design parameters. The results showed that, compared to a single generation system, the multigeneration system led to a 60% and almost 100% increase in the system's energy and exergy efficiencies, respectively. In another study, Ahmadi et al. [8] investigated a trigeneration system comprised of flat plate and photovoltaic/thermal (PV/T) solar collectors, a polymer electrolyte membrane (PEM) electrolyzer, a reverse osmosis (RO) desalination system, and a single effect absorption chiller. Based on a multi-objective optimization, they identified the best operating conditions of the system with an exergy efficiency of 60% and a total cost rate of 154 US$/h. Karellas and Braimakis [9] carried out a thermo-economic analysis on a micro-scale trigeneration system to produce electricity, heating, and cooling. The proposed system included an ORC and a vapor compression refrigeration cycle and was powered by a parabolic trough collector accompanied by a biomass boiler. Results showed that the system overall electric efficiency, electricity output, heating output, and exergy efficiency were 2.38%, 1.42kWe, 53.5kWth, and 7%, respectively. Patel et al. [10] evaluated a trigeneration system consisted of an ORC and cascaded vapor compression and absorption chillers. Energy and exergy analyses showed that the first and second law efficiencies of the system were 79.02% and 46.7%, respectively. In a study by El-Emam and Dincer [11], heliostat field collectors were coupled with a steam Rankine cycle, an RO unit, a single effect H_2O-LiBr absorption chiller, and a PEM electrolyzer to produce electricity, cooling, heating, hydrogen, and fresh water. The system was able to produce 4 MW of electricity, 1.25 kg/h of hydrogen, and 90 kg/s of

fresh water. Anvari et al. [12] conducted a thermodynamic and economic analysis to evaluate a trigeneration system for generating power, cooling, and heating. The system included a 30 MW recuperative gas turbine cycle in which the waste heat in the exhaust gas was used for generating hot water, cooling using an absorption chiller and additional power via an ORC. The results showed that the exergy efficiency of the trigeneration system was 52.8% compared to 51.1% for the gas turbine cycle with heat recovery steam generator. Behnam et al. [13] conducted a thermoeconomic analysis to evaluate the performance of a small trigeneration system operated using geothermal energy for generating electricity, fresh water, and hot water. The system included a geothermal well, an ORC for power generation, a single stage evaporation desalination system, and a single effect H_2O-LiBr absorption heat transformer for generating hot water and supplying heat to the desalination system. The designed system, based on a 100 °C geothermal water, had capacities of generating 161.5 kW power, 0.662 kg/s fresh water, and 246 kW heat. Khanmohammadi and Atashkari [14] carried out a thermoeconomic analysis and applied multi-objective optimization to evaluate a novel trigeneration system for producing electricity, freshwater, and domestic hot water. The system was based on a recuperative gas turbine cycle driven by a biomass gasification process in which the exhaust gas was recovered using an ORC, fresh water using an MED unit, and hot water. The results showed that 163.37 kW power could be generated using the ORC. Also, depending on the gasification temperature, 1,060-1,160 m^3/day freshwater could be produced. Gargari et al. [15] evaluated the performance of a novel multigeneration system based on gas turbine-modular helium reaction (GT-MHR). The authors assessed the system performance from energy, economic, and environmental viewpoints. Under optimum conditions, the multigeneration system could generate 123.59 MW, 0.73 MW, 280.35 MW, 18.14 kg/s, and 0.2432 kg/s of cooling, heating, power, freshwater, and hydrogen, respectively. Zoghi et al. [16] proposed a trigeneration system which combined an ORC and an absorption-compression cooling and power system for waste energy recovery from a diesel engine. The system was designed to generate power, cooling, and domestic hot water. The authors performed an exergoeconomic analysis and a parametric study to evaluate system performance. The net power output and COP of the absorption-compression cooling system were found to be 51.88 kW and 0.6188, respectively. Also, the overall energy and exergy efficiencies were obtained as 75.79% and 44.19%, respectively. Bottarelli and Cannistraro [17] have developed a prototype geothermal heat exchanger for heat pumps to be used in cold climates. Farsi and Dincer [18] developed a multigeneraton system driven by a high-temperature geothermal source for generating power, freshwater, cooling, and hydrogen. The system consisted of a single flash steam cycle, an ORC, a NH_3-H_2O absorption refrigeration, an electrolyzer, a MED, and a MD. The waste heat of the refrigeration system was used to drive the MED and MD units. An increase in the evaporator temperature of the refrigeration system caused a significant increase in the refrigeration performance while it led to a small increase in the MED and MD performance. The authors concluded that the system could generate 165,600 kg/day freshwater. Safari and Dincer [19] proposed a

multigeneration system based on a gas turbine cycle driven by biogas for producing power, freshwater, heating, and hydrogen. In this system, the exhaust heat of the gas turbine cycle was used for additional power generation by an ORC and freshwater production using an MED plant. A part of the generated electricity was used to produce hydrogen using an electrolyzer. The results showed that the multigeneration system had energy and exergy efficiencies of 63% and 40%, respectively.

Natural gas combined cycle power plants are currently accounting for a large portion of power generation capacity in most parts of the world including the US and it is projected that their capacity grows more in the future. Natural gas combined cycle power plans are much cleaner and sustainable than other fossil fuel based power plants. Many efforts have been devoted to improving the technical and economic performance and sustainability of natural gas combined cycle power plants. Some studies demonstrated that inlet air cooling through an absorption chiller, by recovering waste energy from the exhaust stage, can improve the performance of gas turbine combined cycles [20-23]. Other studies evaluated different gas turbine combined cycle configurations and additional waste energy recovery through other cycles such as an ammonia power cycle [24], a CO_2 transcritical power cycle [25], and an ORC [26]. Although the available waste heat in the exhaust stage of the gas turbine cycle is recovered by a steam Rankine bottoming cycle, there are still many possibilities for energy recovery for generating other products.

In this study, different hybrid trigeneration systems based on a gas turbine combined cycle are developed and evaluated for generating electricity, freshwater and cooling for air conditioning. To the best knowledge of the authors, no thorough studies have been presented in the literature to evaluate several hybrid trigeneration systems based on a gas turbine combined cycle and different desalination and chiller systems. The objective of this study is to provide a comprehensive performance evaluation of several hybrid trigeneration system configurations using thermodynamic and economic analysis. The trigeneration systems are based on the hybridization of different desalination and chiller systems to the steam Rankine bottoming cycle. Two desalination technologies evaluated in this study are an MED plant and an RO unit that employs a pressure exchanger energy recovery device. Also, the employed chiller systems in the trigeneration configurations include a double effect H_2O-LiBr absorption chiller (DEABC), a half effect H_2O-LiBr absorption chiller (HEABC) and a vapor compression chiller (VCC) with different working fluids. The specific goal of this study is to identify the optimal hybridization scheme and parameters among different feasible hybrid system configurations. The most significant aspect of these trigeneration systems is that they are based on proven and commercially available technologies. Also, the integration schemes of different cycles are not complex and practically feasible. Therefore, the originality of this study is providing a comparative thermo-economic evaluation of several feasible hybrid trigeneration configurations based on proven technologies and the introduction of the most economical option with the lowest annual cost. The results of this study provide a significant insight into technical and economic aspects of hybrid

trigeneration systems based on gas turbine combined cycle and different desalination and chiller systems.

2. Hybrid trigeneration systems

In this study, different hybrid system configurations are evaluated for trigeneration of power, cooling (air conditioning), and freshwater. To develop the hybrid system configurations, different desalination systems and chiller systems are integrated with a 100,000 kW gas turbine combined cycle (GTCC). A simple regenerative steam Rankine cycle that employs one open feedwater heater is used as the bottoming cycle. Two cooling options are considered to reject the waste heat from the condenser section of the steam Rankine cycle including a dry condenser (air-cooled condenser) and a natural draft wet cooling tower that uses seawater as a cooling medium. Detailed information about wet and dry cooling tower systems used in power cycles can be found in [27, 28]. Two desalination technologies, a multi-effect distillation (MED) and a reverse osmosis (RO) that employs a pressure exchanger energy recovery device, are considered and evaluated in this study. The MED plant employed in this study has a parallel/cross flow configuration which provides a higher productivity for freshwater production than other available configurations [29]. Detailed process descriptions of the MED and RO plants is available in [29]. The chiller systems include a double effect absorption chiller (DEABC), a half effect absorption chiller (HEABC) and vapor compression chiller (VCC) with different working fluids. HEABC configuration is similar in complexity to the DEABC configuration, but it has a substantially lower coefficient of performance (COP). HEABC is a suitable option when the temperature of available heat (dry steam or waste heat) is lower than the minimum temperature required to drive a single effect absorption chiller (SEABC). The main reason for referring to it as half effect is that the COP of a HEABC is almost half of a SEABC while its configurations differs with a SEABC. The detailed process diagrams of different types of absorption chillers are available in [30].

Considering different feasible integrations of these systems, 6 hybrid configurations are evaluated and compared for generating power, cooling (air conditioning), and freshwater. Table 1 lists these hybrid system configurations. For all configurations, the nominal capacity of cooling and freshwater productions are considered 10,000 kW and 20,000 m^3/day, respectively.

Table 1 - Different hybrid trigeneration configurations for generating power, air conditioning and freshwater.

Configuration #	Description
Configuration 1	GTCC with wet cooling tower + DEABC + RO
Configuration 2	GTCC with wet cooling tower + VCC + RO
Configuration 3	GTCC with dry cooling tower + DEABC + RO
Configuration 4	GTCC with dry cooling tower + VCC + RO
Configuration 5	GTCC + DEABC + hybrid MED-RO

The hybrid configurations 1 and 2 are based on a GTCC with a steam bottoming cycle employing a wet cooling tower that uses seawater as a cooling medium. Configurations 1 and 2 differ in terms of their employed chiller technology for air conditioning purposes. Fig. 1 shows the hybrid trigeneration configuration 1 integrating a GTCC that uses wet cooling tower with a DEABC and a RO unit. In configuration 1, a DEABC operates by using the steam extracted from the Rankine cycle. Thus, in addition to steam extraction for the open feedwater heater, another extraction is considered for the DEABC. The amount of steam extracted for driving the DEABC is depending on the air conditioning demand. This configuration also includes an RO to generate freshwater using the electricity generated by the GTCC.

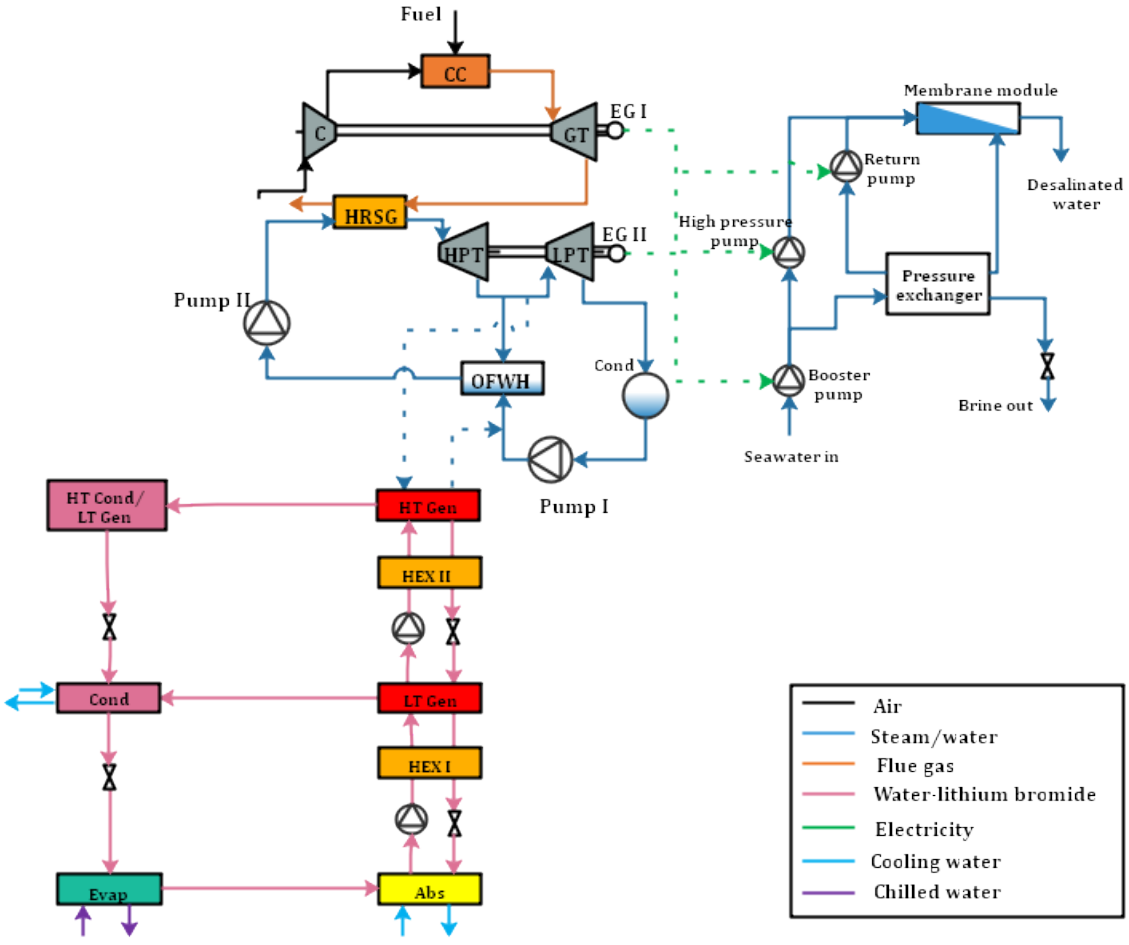

Fig. 1. Hybrid trigeneration configuration 1 integrating a GTCC that uses wet cooling tower with a DEABC and a RO unit.

Configuration 2 is similar to configuration 1 expect it employs a VCC rather a DEABC for generating cooling. In contrast to a DEABC which operates based on thermal energy and has a minimal electricity requirement, an VCC is an electrically driven chiller system. Thus, the VCC does not necessarily need to be co-located with the GTCC like DEABC.

The schematic of the hybrid trigeneration configuration 2 is shown in Fig. S1 in supplementary materials.

The configurations 3 and 4 are similar to configurations 1 and 2, respectively, and their only difference is the use of a dry condenser system in the steam Rankine cycle instead of a wet cooling condenser system. Using a dry condenser demands a different set of design conditions for the GTCC, which also impacts the performance and economics of DEABC, VCC, and RO systems.

Configurations 5 and 6 eliminate the use of any condenser and cooling tower for rejecting the waste heat from the steam Rankine cycle. Fig. 2 shows the hybrid trigeneration configuration 5 integrating a GTCC with a hybrid MED-RO and DEABC. Configuration 5 provides the air conditioning demand using a DEABC by utilizing the steam extracted from the steam Rankine cycle. In configuration 5, the condenser section of the Rankine cycle is replaced with an MED system. Using the available thermal energy in the condensation stage of the Rankine cycle, the MED system can supply a part of freshwater demands. For this purpose, the condensation stage temperature and pressure are set at higher values so that the available steam can meet the thermal requirement of the MED plant. For this study, the condensation stage steam temperature is set at 333K which is a suitable temperature for driving an MED plant. As the available steam is not enough to supply the assigned freshwater demand, the MED system is hybridized with an RO system to supply this demand.

The MED and RO systems are normally hybridized either in parallel or series mode. In this study and for both configurations 5 and 6, the series mode is considered in which the outlet of the feed seawater from the condenser of the MED plant is fed to the RO plant. This hybridization mode has two main benefits. First, it eliminates the need to feed pump power for the RO plant. Second, it improves the performance of the RO unit as the seawater fed to the RO is preheated in the condenser of the MED plant. The reason is that, with an increase in the feed water temperature, the membrane permeability increases leading to a reduction in the pumping power consumption [31].

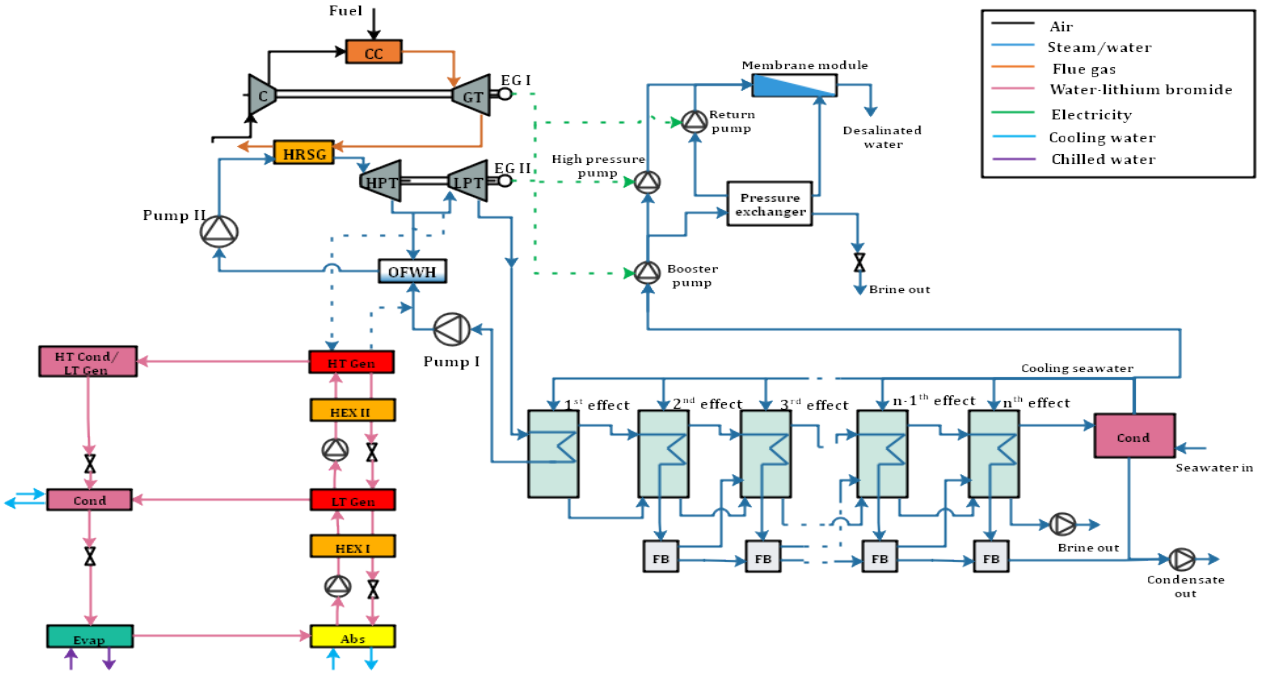

Fig. 2. Hybrid trigeneration configuration 5 integrating a GTCC with a hybrid MED-RO and DEABC.

Fig. 3 shows the hybrid trigeneration configuration 6 integrating a GTCC with a hybrid MED-RO and HEABC. In configuration 6, the Rankine cycle's condenser section is replaced with an HEABC and an MED. A part of the available thermal energy in the condensation stage of the Rankine cycle is used to drive the generators of the HEABC. The rest of the condensation stage's thermal energy is supplied to an MED unit for freshwater production. The temperature remains at 333 K which is suitable for both MED and HEABC systems.

Similar to configuration 5, a hybrid MED-RO system designed to supply the freshwater demand. The replacement of the condenser and cooling tower with the MED and HEABC systems in configurations 5 and 6 causes a significant reduction in the capital cost of the steam Rankine cycle. However, it causes a penalty in the power production and thermal efficiency of the Rankine cycle due to setting a higher condensation temperature and pressure.

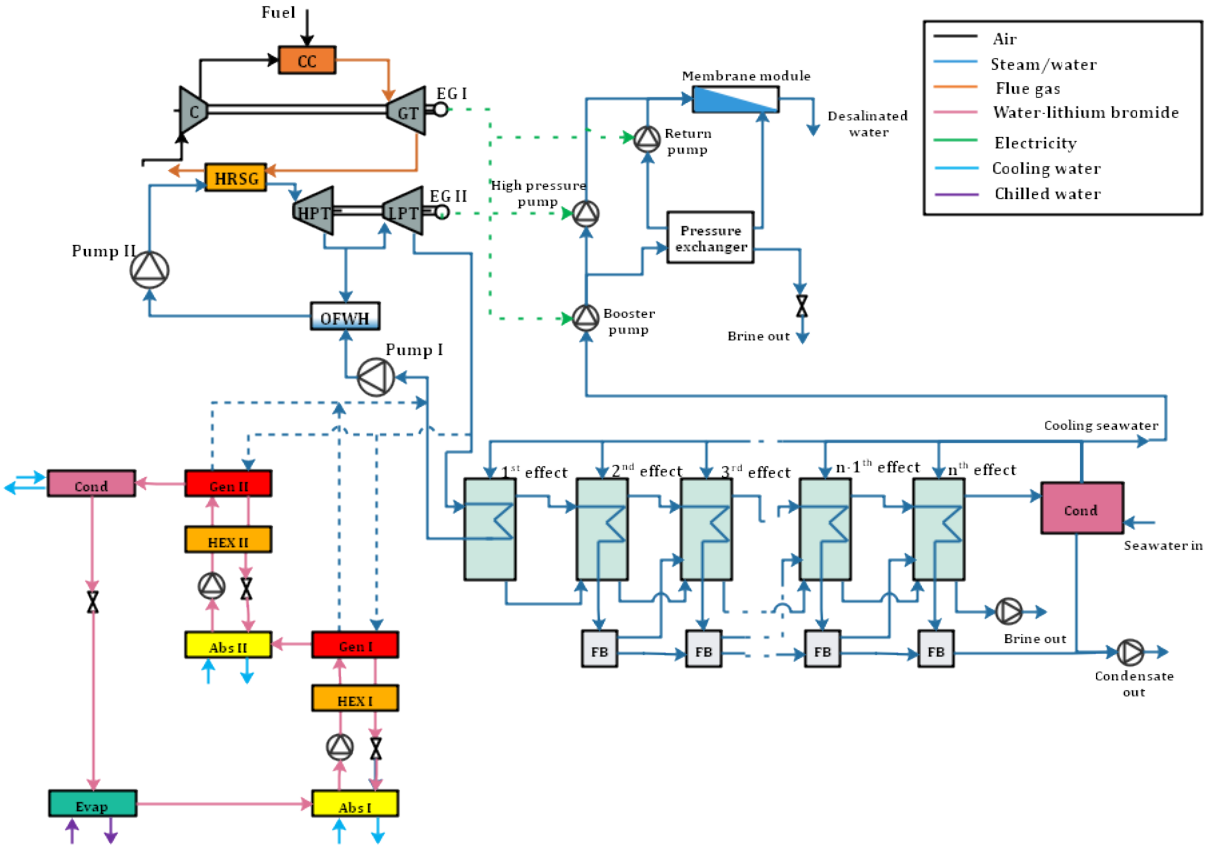

Fig. 3. Hybrid trigeneration configuration 6 integrating a GTCC with a hybrid MED-RO and HEABC.

3. Thermodynamic model

Thermodynamic and economic analyses were carried out to evaluate and compare the performance of the hybrid trigeneration system configurations. Engineering equation solver (EES) was used to simulate and evaluate these hybrid configurations [32].

This section presents the developed thermodynamic models for each sub-system of the hybrid systems while the economic models are presented in Section 4.

The principles of thermodynamics are used to apply the mass and energy balances to different sub-systems and components of the hybrid systems. The models are developed under a steady state steady flow condition with neglecting kinetic, potential, and chemical energies, heat loss in the components and pressure losses in the piping. The thermodynamic models of different systems are presented in Sections 3.1 to 3.4. The thermodynamic models' verification is given in supplementary materials.

3.1. Gas turbine combined cycle

As noted in Section 2, a gas turbine combined cycle (GTCC) is integrated with different chiller and desalination systems to provide the electrical and thermal energy required for driving those systems. A simple regenerative steam Rankine cycle with one open feedwater heater is employed as the bottoming cycle of the gas turbine cycle. The net power output of

the combined cycle is considered 100,000 kW although the gross power is much higher, as a part of the generated electricity by the combined cycle is used for the chiller and desalination systems.

For the Brayton cycle (gas turbine cycle), the net power output ($\dot{W}_{net,Bray}$) and thermal efficiency ($\eta_{th,Bray}$) are calculated using Eqs. (1) and (2) as follows:

$$\dot{W}_{net,Bray} = \dot{m}_{gas}.w_{gas,turb} - \dot{m}_{air}.w_{comp} \quad (1)$$

$$\eta_{th,Bray} = \frac{\dot{W}_{net,Bray}}{\dot{m}_f.LHV.\eta_{cc}} \quad (2)$$

where $\dot{m}_{gas}$ is the mass flow rate of flue gas exiting the gas turbine, and $\dot{m}_{air}$ is the mass flow rate of air entering the compressor. $w_{gas,turb}$ and w_{comp} are the specific works of the gas turbine and compressor, respectively. $\dot{m}_f$ is the mass flow rate of the fuel (pure methane, CH_4), LHV is the fuel lower heating value, and η_{cc} is the efficiency of the combustion chamber.

For the steam Rankine cycle that employs a dry condenser, the net output power ($\dot{W}_{net,Rank}$) and the thermal efficiency ($\eta_{th,Rank}$) are calculated via Eqs. (3) and (4), respectively:

$$\dot{W}_{net,Rank} = \left(\sum_{i=1}^{2} \dot{W}_{steam,turb,i} - \sum_{i=1}^{2} \dot{W}_{pump,i} - \dot{W}_{fan}\right) \quad (3)$$

$$\eta_{th,Rank} = \frac{\dot{W}_{net,Rank}}{\dot{Q}_{HRSG}} \quad (4)$$

$\dot{W}_{fan}$ is the work consumed by the dry condenser's fan calculated using the methodology presented in [33]. Note that when a wet cooling tower is considered or the condenser is replaced by MED or HEABC, $\dot{W}_{fan}$ is equal to zero. However, in those cases, the power required to drive the chillers and desalination are added. $\dot{W}_{steam,turb}$ and $\dot{W}_{pump}$ are calculated using turbine's isentropic efficiency ($\eta_{isen,turb}$) and pump's isentropic efficiency ($\eta_{isen,pump}$) as expressed by Eqs. (5) and (6), respectively:

$$\dot{W}_{steam,turb} = \dot{m}_{steam}(h_{in} - h_{out}) = \dot{m}(h_{in} - h_{out,s})\eta_{isen,turb} \quad (5)$$

$$\dot{W}_{pump} = v_{in}\left(\frac{P_{in} - P_{out}}{\eta_{isen,pump}}\right) \quad (6)$$

$\dot{Q}_{HRSG}$ presented in Eq. (4) is the total heat added to the heat recovery steam generator (HRSG) section.

The HRSG section includes three components of a pre-heater, a boiler, and a superheater which were modeled separately as each has a different form of energy balance. 1% pressure loss was considered for each of these components.

The open feedwater heater was modeled using terminal temperature difference (TTD), defined as the difference between the saturation temperature of the extraction steam and the outlet temperature of feedwater heater.

The dry condenser was designed based on the dry bulb temperature or ambient temperature (T_{amb}) while the wet cooling tower was designed based on the wet bulb temperature (T_{wb}). In this study, a 10K difference is assumed between the ambient temperature and the wet bulb temperature. The heat transfer and pressure drop analyses of the dry condenser were carried out according to the models presented in [33]. For designing the dry condenser, two parameters of initial temperature difference (ITD), and air temperature difference (ATD) were considered. ATD is the difference between the inlet and outlet air temperatures of the dry condenser. ITD is the difference between the condensation temperature and the ambient temperature.

The wet cooling tower was designed based on three design parameters of approach, range, and TTD. Approach is defined as the temperature difference between the water leaving the cooling tower and T_{wb}. While range is defined as the difference between the inlet and outlet temperatures of the cooling water. For a wet-cooled condenser, TTD is the difference between the steam saturation temperature and the outlet cooling water temperature.

Seawater has different thermophysical properties than freshwater which impact the mass and heat transfer processes in the wet cooling tower. Therefore, the correlations presented by Sharqawy et al. [34] were utilized for calculating the thermophysical properties of seawater.

The inputs used for the design of the GTCC are given in Table 2.

Table 2 - Input design parameters for the GTCC.

Parameter	Value
ΔP_{cc}	4%
η_{comp}	0.85
η_{turb}	0.87
η_{cc}	0.98
$\eta_{elect-gen}$	0.98
$\eta_{isen,turb}$	0.85
$\eta_{isen,pump}$	0.80
$P_{turb,int,Rank}$	8,000 kPa
$T_{turb,int,Rank}$	793 K
ATD	10 K
ITD	25 K

Approach	5 K
Range	10 K
TTD_{Cond}	3 K
$\dot{W}_{net}$	100,000 kW

3.2. Water-lithium bromide absorption chillers and compression chiller

The specific assumptions used to model and evaluate the performance of the absorption and compression chillers are: (1) For both absorption and compression chillers, the refrigerants leaving absorber, condenser, and evaporator are saturated, (2) The process inside the expansion valves is isenthalpic, (3) For the double effect absorption chiller, the pinch temperature difference in the internal heat exchanger processes between HTC and LTG is assumed 5 °C, (4) For absorption chillers, the temperatures of absorber and condenser are equal, and (5) For both double effect and half effect absorption chillers, the inlet and outlet temperatures of cooling water for absorber and condenser are equal.

The performance of the chillers is evaluated based on the coefficient of performance (COP), defined as a ratio of the generated cooling effect in the evaporator ($\dot{Q}_{evap}$) to the input thermal and/or electrical energy required to run the chiller.

The COP of the absorption chillers is calculated as follows:

$$COP_{ABC} = \frac{\dot{Q}_{evap,ABC}}{\dot{Q}_{gen} + \sum \dot{W}_{pump,ABC}} \quad (7)$$

where $\dot{Q}_{gen}$ is the thermal energy, in the form of dry steam, supplied to the generators of the absorption chiller cycles. For the HEABC, $\dot{Q}_{gen}$ is the summation of thermal energy supplied to both high-temperature generator ($\dot{Q}_{HTgen}$) and low-temperature generator ($\dot{Q}_{LTgen}$). $\dot{W}_{pump,ABC}$ represents the powers consumed by absorption chiller's pumps.

For the vapor compression chiller, the COP is calculated as expressed by Eq. (8):

$$COP_{VCC} = \frac{\dot{Q}_{evap,VCC}}{\dot{W}_{comp}} \quad (8)$$

where $\dot{W}_{comp}$ is the work required to the drive the compressor, calculated using Eq. (9) as follows:

$$\dot{W}_{comp} = \dot{m}(h_{out,s} - h_{in})/\eta_{isen,comp} = \dot{m}(h_{out} - h_{in}) \quad (9)$$

where $\eta_{isen,comp}$ is the isentropic efficiency of the compressor considered equal to 0.7. Also, the electrical and mechanical efficiencies of the compressor were considered as constant value of 0.95 each.

For chiller systems, only a wet cooling condenser was considered to achieve a more favorable performance. Table 3 presents the main parameters used as inputs to model the absorption and compression chillers.

The inlet and outlet temperatures of chilled water were considered to be 8 K and 3 K higher than the evaporator temperature, respectively.

Table 3 - Input design parameters for absorption and compression chillers.

Parameter	Value
T_{evap}	280 K
ε_{SHX}	0.75
Approach	3 K
Range	5 K
TTD_{Cond}	3 K
$\eta_{iesn,comp}$	0.7
$\eta_{elect,comp}$	0.95
$\eta_{mech,comp}$	0.95

3.3. Multi-effect distillation

As noted, a parallel/cross flow MED configuration is considered in this study owing to its higher productivity. In this configuration, the feed seawater is equally distributed to all effects. The steam at 333 K coming from the condensation stage of the Rankine cycle is supplied to the first effect of the MED plant. To simulate the MED plant's performance, it is assumed that the distillate generated in all effects is salt-free, and the temperature difference (ΔT) between all effects is equal. Moreover, the non-equilibrium allowance and any heat loss from each component to the surroundings is neglected.

In this study, the productivity or performance of the MED plant is evaluated using gain output ratio (GOR), defined as a ratio of the mass flow rate of the total distillate, or freshwater, generated in all effects ($\dot{m}_D$) to the mass flow rate of steam ($\dot{m}_s$) supplied to the 1st effect [35]. GOR is expressed by Eq. (10) as follows:

$$GOR = \frac{\dot{m}_D}{\dot{m}_s} \tag{10}$$

Although an MED plant is a thermally driven desalination system, it requires some pumping units for the feed seawater, distillate product, brine reject, and chemical dosing [32]. This pumping power requirement, or specific power consumption of the MED plant, is normally considered 1.5-2.5 kWh/m^3. In this study, a value of 2.0 kWh/m^3 is assumed. For configurations 5 and 6, depending on the MED capacity, the total MED's pumping power requirement ($\dot{W}_{MED}$) is calculated as follows:

$$\dot{W}_{MED} = \dot{m}_D \times 2.0 \times 3.6 \tag{11}$$

The factor of 3.6 was added to convert $\dot{m}_D$ from kg/s to m^3/h.

The design parameters of the MED plant are presented in Table 4.

Table 4 -Input data for simulation of the MED plant.

Parameter	Value
Number of effects	4, 6, 8
Inlet steam temperature	333 K
Top brine temperature	330 K
Last effect brine temperature	311 K
BPE	0.8
T_{SW}	298 K
T_F	308 K
X_F	40,000 ppm

3.4. Reverse osmosis

For the simulation of the RO plant, a model based on a previous study were developed [36]. The mass flow rate of generated distillate ($\dot{m}_D$) by the RO plant and its salinity (X_D) are calculated using Eqs. (12) and (13) as follows [36]:

$$\dot{m}_D = \dot{m}_F.RR \tag{12}$$

$$X_D = X_F.(1 - SR) \tag{13}$$

where RR is the recovery ratio, and SR is the salt rejection ratio.

The mass flow rate and salinity of the rejected brine from the RO system ($\dot{m}_B$ and X_B) are determined as presented by Eqs. (14) and (15), respectively [36:

$$\dot{m}_B = \dot{m}_F - \dot{m}_D \tag{14}$$

$$X_B = \frac{\dot{m}_F.X_F - \dot{m}_D.X_D}{\dot{m}_B} \tag{15}$$

The number of required elements for the RO unit is calculated by Eq. (16) as follows [37, 38]:

$$N_E = \frac{\dot{Q}_P}{f.\,A_{memb}} \tag{16}$$

where $\dot{Q}_P$ is the permeate flow rate in m^3/h, f is the average flux of the membrane, and A_{memb} is the membrane area. In this study, a membrane type of FTSW30HR-380 is considered for the RO plant.

Then the number of pressure vessels (N_{PV}) can be determined by Eq. (17) as follows [37, 38]:

$$N_{PV} = \frac{N_E}{N_{E,PV}} \quad (17)$$

where $N_{E,PV}$ is the number of elements connected in series in each pressure vessel.

The required power for each pump of the RO system is generally expressed by Eq. (18) as follows:

$$\dot{W}_{pump,RO} = \frac{\dot{m}_F \Delta P}{\rho \eta_{pump,RO}} \quad (18)$$

The total pump work of the RO unit is the sum of works required for the feed pump ($\dot{W}_{feed\ pump,RO}$), high pressure pump ($\dot{W}_{HP\ pump,RO}$) and booster pump ($\dot{W}_{booster\ pump,RO}$).

For the pressure exchanger (PEX) device, Eq. (19) is applied based on its efficiency (η_{PEX}) [39, 40]:

$$\eta_{PEX} = \frac{\dot{m}_F.P_{F,out} + \dot{m}_B.P_{B,out}}{\dot{m}_F.P_{F,in} + \dot{m}_B.P_{B,in}} \quad (19)$$

where $P_{F,in}$ and $P_{F,out}$ are the pressures of inlet and outlet feed seawater, respectively while $P_{B,in}$ and $P_{B,out}$ are the pressures of inlet and outlet brine, respectively.

Table 5 presents the input parameters for the RO unit with PEX.

Table 5- Design parameters for the RO unit with PEX.

Parameter	Value
A_{memb}	35.4 m^2
FF	0.85
$N_{E,PV}$	7
T_F	35 °C
X_F	40,000 ppm
η_{PEX}	0.90
$\eta_{pump,RO}$	0.75

4. Economic model

This section presents the economic models used to evaluate and compare the economic performance of the hybrid trigeneration configurations. For each sub-system, three different economic parameters of annual capital cost (ACC), annual operating cost (AOC), and levelized cost of useful products are calculated. For each system, the economic model and data from previous studies were used.

The economic performance of the gas turbine combined cycle was evaluated using the same methodology, cost functions, and cost data as those utilized in the previous studies

of the authors [41, 42]. For the absorption and compression chillers, the economic model, cost functions, and data used in a previous study were used [45].

To calculate the investment cost of the dry cooling system including the heat exchanger unit, fans, and motor, structure and piping, the following cost function as expressed by Eq. (21) is used [44]:

$$C_{Dry\ cooling} = (0.7434 \times (ITD)^2 - 48.721 \times ITD + 1017.1) \times \dot{W}_{net,Rank} \qquad (20)$$

This cost function calculates the cost of the dry cooling system in Euro so currency conversion was used to convert the cost to US Dollar.

The investment cost of the wet cooling system includes the cost of the wet cooled condenser and the natural draft cooling tower. The cost of condenser is calculated by Eq. (21) as follows [45]:

$$C_{cond} = 32{,}800 \times C_f \times \left(\frac{A}{80}\right)^{0.68} \qquad (21)$$

Use of seawater as a cooling medium raises some corrosion concerns in the wet cooling system. To avoid and minimize such concerns, proper materials should be selected. In this study, carbon steel is used in the shell side and stainless steel is used in the tube side of the condenser heat exchanger. Thus, a material correction factor (C_f) of 1.7 is added to include the effect of adding stainless steel [45].

The cost of cooling tower is calculated using Eq. (22) as follows [43]:

$$C_{cooling\ tower} = b_1 \times \dot{m}_{cw}^{b_2} \times 10^{b_3 \times Y \times Z + b_4 \times A + b_5 \times R + b_6} \qquad (22)$$

The values of coefficients b_1-b_6 are found [43]. Also, Y and Z are defined using Eqs. (23) and (24), respectively [43]:

$$Y = T_{cw,in} - T_{wb,\ air,in} \qquad (23)$$

$$Z = T_{cw,out} - T_{cw,in} \qquad (24)$$

$T_{cw,in}$ is the cooling water temperature at the outlet of the tower or inlet of the condenser and $T_{cw,out}$ is the cooling water temperature at the inlet of the tower or outlet of the condenser. Also, $T_{wb,\ air,in}$ is the wet bulb temperature of the inlet air to the tower.

To calculate the cost of all heat exchangers including those of the absorption chillers, the compression chiller, and the condenser of the wet cooling system, their heat transfer area (A) is calculated using Eq. (25) as follows:

$$A = \frac{\dot{Q}}{U\Delta T_{LMTD}} \quad (25)$$

where U and ΔT_{LMTD} are heat transfer coefficient and logarithmic mean temperature difference, respectively.

Detailed economic models based on both capital and operating costs of the MED and RO plants were used to evaluate their economics and calculate the levelized cost of water (LCOW) in different trigeneration configurations. For both MED and RO plants, the capital costs consist of direct and indirect costs which each includes several terms. The operating cost includes different terms such as the costs of maintenance and replacement, labor, pre-treatment, insurance cost, and cost of electricity. For all sub-systems of the trigeneration configurations including the RO and MED plants, the specific cost of electricity is the levelized cost of electricity (LCOE) generated by the gas turbine combined cycle. Tables S1 and S2 in supplementary materials present the capital investment cost and operating cost of the RO plant, respectively. The used equation and data to calculate the capital investment cost and operating cost of the MED plant are presented in Tables S3 and S4 of the supplementary materials, respectively.

The used cost equations and data for different components are related to different years. To make the economic analysis relevant and accurate, the chemical engineering plant cost index (CI) was used to update the costs to the year 2018.

After calculating the total investment cost (TIC), the ACC of each system can be calculated as follow:

ACC is a function of the TIC and the capital recovery factor (*CRF*) calculated by Eq. (28):

$$ACC = TIC \times CRF \quad (26)$$

CRF is a function of lifetime of the system and discount rate which are assumed for all systems to be 25 years and 0.07, respectively.

The levelized cost of electricity, water and cooling (LCOE, LCOW and LCOC) are calculated using Eqs. (27), (28) and (29), respectively:

$$LCOE = \frac{ACC_{GTCC} + AOC_{GTCC}}{EP_{annual}} \quad (27)$$

$$LCOW = \frac{ACC_{MED/RO} + AOC_{MED/RO}}{FWP_{annual}} \quad (28)$$

$$LCOC = \frac{ACC_{ABC/VCC} + AOC_{ABC/VCC}}{CP_{annual}} \quad (29)$$

where EP_{annual}, FWP_{annual} and CP_{annual} are the annual electricity production, freshwater production and cooling production, respectively.

5. Results and discussion

The primary analysis and results show that the capital and annual costs of the gas turbine cycle is significantly higher than desalination and chiller systems. Although the objective of this work is not to optimize the systems, a simple optimization was conducted using EES to achieve the minimum LCOE for the combined cycle. The turbine inlet temperature of the Brayton cycle ($TIT_{Brayton}$) and compressor pressure ratio (PR) were considered as decision variables. The assigned ranges of search for $TIT_{Brayton}$ and PR are between 1373 K and 1573 K and between 8 and 12, respectively. Table 6 presents the optimum values of PR and $TIT_{Brayton}$ obtained for different combined cycle configurations. It is observed that a relatively higher PR and $TIT_{Brayton}$ is obtained for configurations 3 and 4 that employs a dry cooling system for the Rankine cycle. Note that for configurations 5 and 6, due to the same type of configuration and energy recovery, which replaces cooling tower with other sub-systems, the optimum values of PR and $TIT_{Brayton}$ are almost the same. For all other sub-systems, the input parameters were assigned based on some preliminary analysis and the findings from previous studies to ensure all the sub-systems have a favorable thermodynamic and economic performance.

Table 6- Optimum values of PR and $TIT_{Brayton}$ for different combined cycle configurations.

Configuration #	PR	$\boldsymbol{TIT_{Brayton}(K)}$
Configuration 1	12.2	1495
Configuration 2	12.0	1493
Configuration 3	13.2	1500
Configuration 4	12.9	1496
Configuration 5	12.3	1494
Configuration 6	12.4	1494

As noted, different working fluids were evaluated for the vapor compression chiller (VCC) to determine the most suitable fluid. Five environmentally friendly working fluids of R600, R290, R717, R1234yf and R1234ze(E) were selected for this study.

Table 7 shows the thermodynamic and economic results obtained for these five working fluids considering the inputs given in Table 3 and the cost of electricity of $0.07/kWh. The obtained results demonstrate that R717 is the most suitable working fluid from both thermodynamic and economic viewpoints. Therefore, for the rest of the paper, R717 is considered as the working fluid in the VCC.

Table 7- Thermodynamic and economic comparisons between different working fluid used for the VCC.

Working fluid	COP	TAC ($\$/year$)	$LCOC$ ($\$/ton-hr$)
R600	5.970	1,063,000	0.0748
R290	5.671	1,080,500	0.0760
R717	5.994	990,700	0.0697
R1234yf	5.558	1,127,100	0.0793
R1234ze(E)	5.782	1,091,000	0.0767

Table 8 presents the thermodynamic results of the gas turbine combined cycle for different hybrid trigeneration configurations.

The results include the thermodynamic efficiency of the Brayton cycle, Rankine cycle and gas turbine combined cycle (η_{Bray}, η_{Rank} and η_{GTCC}), the gross power generated by the Brayton and Rankine cycles ($\dot{W}_{gross,Bray}$ and $\dot{W}_{gross,Rank}$) and the consumed power by dry condenser's fan ($\dot{W}_{fan}$).

Table 8 - Thermodynamic results of the gas turbine cycle for different hybrid trigeneration configurations.

Configuration #	η_{Bray}	η_{Rank}	η_{GTCC}	$\dot{W}_{gross,Bray}$ (kW)	$\dot{W}_{gross,Rank}$ (kW)	$\dot{W}_{fan}$ (kW)
1	0.3275	0.3276	0.4535	72,203	30,252	-
2	0.3269	0.3501	0.4552	71,814	32,309	-
3	0.3338	0.2953	0.4416	75,584	26,871	1,097
4	0.3321	0.3150	0.4412	75,264	28,859	1,283
5 (4-effect MED)	0.3285	0.3075	0.4457	73,717	28,318	-
5 (6-effect MED)	0.3285	0.3075	0.4461	73,645	28,288	-
5 (8-effect MED)	0.3285	0.3075	0.4465	73,577	28,260	-
6 (4-effect MED)	0.3285	0.3289	0.4540	72,369	29,731	-
6 (6-effect MED)	0.3285	0.3289	0.4543	72,318	29,709	-
6 (8-effect MED)	0.3285	0.3289	0.4546	72,270	29,690	-

The lowest η_{Rank} is obtained for configuration 3 because of the significant penalty in the power and thermal efficiency due to the implementation of dry condenser and DEABC. Employment of the dry condenser demands a high condensation temperature and pressure leading to a power and efficiency penalty. Also, when DEABC is integrated, a part of the steam that goes to the lower pressure turbine is extracted for supplying the thermal demands of the DEABC. This means less steam remains to be expanded in the lower pressure turbine for electricity generation leading to a penalty in the power and efficiency. This is the main reason that configuration 3 has a lower η_{Rank} than configuration 4. The highest η_{Rank} is obtained for configuration 2 because no absorption chiller or MED systems are integrated to the Rankine cycle. Both VCC and RO systems are electrically driven, and as a result, they can be located

anywhere and the required electricity can be sent directly to these systems. According to Table 8, the highest and the lowest η_{GTCC} are obtained for configurations 2 and 4 with the values of 0.4552 and 0.4412, respectively. Configurations 3-6 experience a substantial penalty in power and efficiency due to employment of a dry condenser or replacement of a condenser with an MED or MED and HEABC.

For configurations 5 and 6, three different cases are considered for the MED plant by setting its number of effects to 4, 6, and 8. The results for configurations 5 and 6 demonstrate that increasing the number of effects for the MED plant causes an increase in the η_{GTCC}. The reason is with an increase in the number of effects, the productivity of the MED plant increases meaning less freshwater is produced by the RO unit. As the MED plant has a lower electrical requirement, or specific power consumption, than the RO plant, increasing the number effects causes a reduction in the gross power that should be generated to produce the same amount of freshwater; therefore, the η_{GTCC} increases. Among all configurations, the highest $\dot{W}_{gross,Bray}$ and the lowest $\dot{W}_{gross,Rank}$ are obtained for configurations 3 and 4 because of the dry condenser.

Thermodynamic results of different desalination and chiller systems for all hybrid trigeneration configurations are presented in Table 9. These results include the power consumed by the MED, RO and VCC systems ($\dot{W}_{MED}$, $\dot{W}_{RO}$ and $\dot{W}_{VCC}$), the freshwater production by the MED and RO plants (FWP_{MED} and FWP_{RO}), the steam mass flow rate supplied to the generator(s) of the absorption chillers ($\dot{m}_{gen,ABC}$), and the COP of the absorption and compression chillers. With increasing the number of effects of the MED plant (configurations 5 and 6), the freshwater production capacity increases leading to an increase in the $\dot{W}_{MED}$. As observed and expected, $\dot{W}_{MED}$ values are lower for configuration 6 due to the less freshwater production capacity of the MED plants than the MED plants in configuration 5. The reason is that a part of the steam in the condensation stage of the Rankine cycle is used by the HEABC; thus, less steam remains for the MED plant leading to lower freshwater production capacity and pumping power consumption by the MED plants. $\dot{W}_{VCC}$ is the same for both configurations 2 and 4 due to the same design parameters and cooling capacity.

The results show that a large portion of the nominal freshwater production capacity (20,000 m^3/day) can be generated using the available heat in the condensation stage of the Rankine cycle. For configuration 5, the amounts of freshwater production by the MED plant (FWP_{MED}) are 7,611 m^3/day, 11,051 m^3/day, and 14,265 m^3/day, respectively, which are 38.1%, 55.3% and 71.33% of the nominal freshwater capacity. For configuration 6, the values of FWP_{MED} are 5,436 m^3/day, 7,876 m^3/day, and 10,161m^3/day, respectively, contributing to 27.18%, 39.38% and 50.81% of the total freshwater capacity.

It is observed that $\dot{m}_{gen,ABC}$ values of the DEABC for configurations 1, 3, and 5 are very close. The small differences are because of the small change in the temperature of the steam

extracted for the DEABC. The reason for having extracted steam at different temperatures is that the thermodynamic states of the combined cycle vary when the Rankine cycle's cooling system is changed. As seen, $\dot{m}_{gen,ABC}$ for the HEABC (configuration 6) is 10.5 kg/s which is substantially higher than that of the DEABC. The reason is due to significantly lower COP of the HEABC compared to the DEABC. COP for the VCC (5.994) is more than four times higher than the DEABC and almost fifteen times higher than the HEABC.

Table 9- Thermodynamic results of desalination and chiller systems for different hybrid trigeneration configurations.

Configuration #	$\dot{W}_{MED}$ (kW)	$\dot{W}_{RO}$ (kW)	$\dot{W}_{VCC}$ (kW)	FWP_{MED} (m^3/day)	FWP_{RO} (m^3/day)	$\dot{m}_{gen,ABC}$ (kg/s)	COP
1	-	2455	-	-	20,000	3.552	1.370
2	-	2455	1668	-	20,000	-	5.994
3	-	-	-	-	20,000	3.605	1.371
4	-	2455	1668	-	20,000	-	5.994
5 (4-effect MED)	634	1401	-	7,611	12,389	3.606	1.371
5 (6-effect MED)	921	1012	-	11,051	8,949	3.606	1.371
5 (8-effect MED)	1189	649	-	14,265	5,735	3.606	1.371
6 (4-effect MED)	453	1647	-	5,436	14,564	10.5	0.404
6 (6-effect MED)	656	1371	-	7,876	12,124	10.5	0.404
6 (8-effect MED)	847	1113	-	10,161	9,839	10.5	0.404

Table 10 presents the annual capital cost (ACC) and annual operating cost (AOC) of different systems for different hybrid trigeneration configurations. It also shows the total annual cost (TAC_{total}) of each hybrid system configuration. As expected, the annual costs of the gas turbine combined cycle are significantly higher than other systems. The TAC of the gas turbine combined cycle for different hybrid configuration is between 84.5% (configuration 6 with 8-effect MED) and 90.6% (configuration 3) of the total TAC of hybrid system configurations.

The lowest ACC of the combined cycle (ACC_{GTCC}) is obtained for configuration 5 with 8-effect MED ($11,962,000/year) and the highest ACC_{GTCC} is obtained for configuration 4 ($13,467,000/year). In configuration 5, the condenser of the Rankine cycle is eliminated and replaced with an MED plant leading to a significant reduction in the capital cost. While in configuration 4, the Rankine cycle has a dry cooling system which is very expensive. For both configurations 5 and 6, the ACC of the MED plant increases by increasing the number of effects due to an increase in the heat transfer areas. Also, the AOC increases because the freshwater production capacity increases by having a higher number effects in the MED. As a result, the pumping power needed for the MED plant increases, leading to a rise in the AOC_{MED}.

For configurations 1-4, there is a slight difference between the values of AOC_{RO} while the ACC_{RO} values are constant due to the same size of the RO unit in each hybrid system configuration. The AOC_{RO} varies slightly because of the change in the cost of electricity

generated by the gas turbine combined cycle in each hybrid system and supplied to the RO unit. A comparison of configurations 1-4 with configurations 5 and 6 shows the TAC of the hybrid MED-RO systems in configuration 5 and 6 is much higher than the single RO unit (configurations 1-4). However, configurations 5 and 6 benefit from the lower ACC_{GTCC} due to the elimination of condenser and cooling tower. It is observed that the ACC of HEABC (ACC_{ABC}) in configuration 6 is substantially higher than the ACC of DEABC (ACC_{ABC}) in configurations 1, 3, and 5. This is mainly due to a substantially lower COP of the HEABC than DEABC leading to larger components while the number of components is almost the same. Increasing the steam temperature supplied from the condensation stage of the Rankine cycle could decrease the ACC and AOC of HEABC. However, this occurs at the price of lower η_{Rank} and higher ACC_{GTCC} and AOC_{GTCC}. It is also observed that while the ACC_{VCR} is almost half of ACC_{ABC} of DEABC, the AOC_{VCR} is almost nine times higher. This leads to a significantly higher TAC for the VCC than DEABC demonstrating that the air conditioning using the DEABC is more beneficial than the VCC system. Finally, the results of Table 10 show that the lowest TAC_{total} is obtained for configuration 1 ($49,279,000/year) followed by configuration 2 ($49,867,000/year). While the highest TAC_{total} is obtained for configuration 5 that employs an MED plant with 8 effects ($52,413,000/year). This indicates that configuration 1 has 5.98% less TAC_{total} than configuration 5 with an 8-effect MED unit. Thus, configuration 1 can be introduced as the more suitable hybrid configuration for trigeneration of power, air conditioning, and freshwater. Obviously, increasing the freshwater and air conditioning capacities increases the difference between the TAC of different hybrid configurations. Employing a 4-effect MED plant in configurations 5 and 6 is the more suitable option as increasing the number of effects leads to an increase in the TAC_{total}. It is observed that both configurations 5 and 6 that employ a 4-effect MED plant have a substantially lower TAC_{total} than configurations 3 and 4. This demonstrates that in case of some technical difficulties in implementing a wet cooling tower that uses seawater, configuration 5 may be the more suitable option for trigeneration.

Table 10 -Annual costs of different systems for different hybrid configurations

Configuration #	ACC_{GTCC} $(\frac{\$}{year})$	AOC_{GTCC} $(\frac{\$}{year})$	ACC_{MED} $(\frac{\$}{year})$	AOC_{MED} $(\frac{\$}{year})$	ACC_{RO} $(\frac{\$}{year})$	AOC_{RO} $(\frac{\$}{year})$	ACC_{ABC} $(\frac{\$}{year})$	AOC_{ABC} $(\frac{\$}{year})$	ACC_{VCC} $(\frac{\$}{year})$	AOC_{VCC} $(\frac{\$}{year})$	TAC_{total} $(\frac{\$}{year})$
1	12,287,000	32,205,000	-	-	1,932,000	2,283,000	491,000	81,000	-	-	49,279,000
2	12,549,000	32,148,000	-	-	1,932,000	2,289,000	-	-	291,000	658,000	49,867,000
3	13,158,000	33,184,000	-	-	1,932,000	2,330,000	475,000	78,000	-	-	51,157,000
4	13,467,000	33,266,000	-	-	1,932,000	2,340,000	-	-	291,000	683,000	51,979,000
5 (4-effect MED)	11,982,000	32,643,000	1,705,000	842,000	1,242,000	1,365,000	475,000	78,000	-	-	50,332,000
5 (6-effect MED)	11,972,000	32,613,000	2,752,000	1276,000	935,000	988,000	475,000	78,000	-	-	51,089,000
5 (8-effect MED)	11,962,000	32,585,000	4,259,000	1,783,000	635,000	636,000	475,000	78,000	-	-	52,413,000
6 (4-effect MED)	12,071,000	32,133,000	1,333,000	622,000	1,431,000	1,596,000	1,140,000	186,000	-	-	50,512,000
6 (6-effect MED)	12,064,000	32,111,000	2,154,000	944,000	1,219,000	1,330,000	1,140,000	186,000	-	-	51,148,000
6 (8-effect MED)	12,057,000	32,091,000	3,343,000	1,330,000	1,015,000	1,081,000	1,140,000	186,000	-	-	52,243,000

As TAC_{total} of the hybrid trigeneration configurations 1 and 2 are more close to each other than any other configurations, it is worthwhile to further compare these two configurations when the freshwater and air conditioning demands change. Table 11 provides a comparison between configurations 1 and 2 in terms of TAC_{total} (\$/year) for different cooling and freshwater demands. Note that the typical size of many commercially available H_2O-LiBr absorption chillers is around 5,000 kW [46]. Thus, to make a fair comparison and more accurate economic analysis, for the analysis of Table 11 and the rest of the paper, it is assumed that one or multiple 5,000 kW absorption/compression chillers are employed depending on the desired air conditioning capacity.

These results confirm that configuration 1 is the more economical trigeneration configuration under different cooling and freshwater demands. Note that these two configurations are similar and the only difference is the use of different cooling technology for air conditioning purposes. At higher cooling demands, a higher difference between TAC_{total} of the configurations is observed because of a significant increase in the AOC of the VCC cycle used in configuration 2. The highest difference in TAC_{total} is 1,038,000/year obtained for cooling demand of 20,000 kW and freshwater demand of 20,000 m^3/day.

Table 11- Comparison between TAC_{total} (\$/year) of configurations 1 and 2 for different cooling and freshwater demands

Demands	Configuration 1	Configuration 2
5,000 kW/20,000 m^3/day	48,841,000	49,122,000

10,000 kW/20,000 m^3/day	49,427,000	49,965,000
15,000 kW/20,000 m^3/day	50,012,000	50,799,000
20,000 kW/20,000 m^3/day	50,596,000	51,634,000
10,000 kW/10,000 m^3/day	46,926,000	47,455,000
10,000 kW/20,000 m^3/day	49,427,000	49,965,000
10,000 kW/30,000 m^3/day	51,891,000	52,436,000
10,000 kW/40,000 m^3/day	54,337,000	54,889,000

Table 12 presents the values of levelized cost of different useful products including electricity, freshwater using MED, RO and hybrid MED-RO and cooling using ABC or VCC for all hybrid configurations. The levelized costs are directly related to the TAC so that for the systems with a higher TAC, the expectation is to have higher levelized costs. The lowest LCOE is obtained for configuration 6 that employs an 8-effect MED ($0.0643/kWh) while the highest LCOE is found for configuration 4 ($0.0681/kWh). The reason is that configuration 4 has a dry condenser system while in configuration 6, the condenser and the cooling tower is replaced with an MED plant and an HEABC plant. Configuration 6 shows a slightly lower LCOE than configuration 5. This is due to the fact that in configuration 5, the condenser is only replaced with an MED plant, and as a result, more electricity is required to drive the MED plant which has a higher capacity than the MED pant of configuration 6. Also, configuration 5 employs a DEABC which causes some power penalty due to the use of steam from an extraction line. The results of Table 12 demonstrate that the $LCOW_{MED}$ is much higher than $LCOW_{RO}$ due to higher capital cost of an MED plant compared to an RO plant. An increase in the number of effects of an MED plant leads to an increase in $LCOW_{MED}$ due to a substantial increase in the heat transfer areas and their costs. Note that an increase in the number of effects increases the freshwater productivity and demanding more electricity to drive the MED plant. This leads to a rise in AOC. An increase in the number of effects is beneficial when steam as an input thermal energy is purchased to drive an MED; thus, a trade-off is normally found between the higher number of effects and the cost of purchasing steam, as the main part of the AOC.

665 It is observed that the hybrid MED-RO systems employed in configurations 5 and 6
666 have a higher combined LCOW than the $LCOW_{RO}$ of configurations 1-4. A slight difference in
667 the $LCOW_{RO}$ of configurations 1-4, despite the same freshwater capacity of the RO unit, is
668 due to the difference in the LCOE of these configurations used as the cost of electricity to run
669 the RO plants. This is due to setting a steam temperature of 333 K supplied to the generators
670 of HEABC resulting in a higher $LCOC_{ABC}$. Setting a higher value for the steam temperature
671 causes a reduction in the $LCOC_{ABC}$ of the HEABC; however, it leads to a greater power penalty
672 in the Rankine cycle and subsequently an increase in the TAC of the gas turbine combined
673 cycle.
674
675 **Table 12-** Levelized cost of different useful products for different hybrid configurations

Configuration #	$LCOE$ $(\frac{\$}{kWh})$	$LCOW_{MED}$ $(\frac{\$}{m^3})$	$LCOW_{RO}$ $(\frac{\$}{m^3})$	$LCOW_{MED+RO}$ $(\frac{\$}{m^3})$	$LCOC_{ABC}$ $(\frac{\$}{ton-hr})$	$LCOC_{VCC}$ $(\frac{\$}{ton-hr})$
1	0.06478	-	0.7219	-	0.0402	-
2	0.06508	-	0.7227	-	-	0.0668
3	0.06748	-	0.7298	-	0.0389	-
4	0.06805	-	0.7315	-	-	0.0685
5 (4-effect MED)	0.06598	1.146	0.7206	0.8825	0.0389	-
5 (6-effect MED)	0.06492	1.248	0.7358	1.0189	0.0389	-
5 (8-effect MED)	0.06486	1.451	0.7586	1.2522	0.0389	-
6 (4-effect MED)	0.06426	1.231	0.7117	0.8529	0.0930	-
6 (6-effect MED)	0.06432	1.347	0.7198	0.9667	0.0930	-
6 (8-effect MED)	0.06428	1.575	0.7295	1.1592	0.0930	-

676
677 It is interesting to examine the effect of a change in these capacities on the
678 thermodynamic and economic performances of configuration 1. Table 13 presents the effect
679 of change in the cooling and freshwater demands on the performance of configuration 1. Due
680 to using one or multiple 5,000 kW absorption chillers, an increase in the absorption chiller
681 capacity does not have any impact on the LCOC, and as a result, the related results are not
682 presented in Table 11. According to Table 13, an increase in the cooling and freshwater
683 capacities cause a decrease in η_{GTCC} and an increase in LCOE. $LCOW_{RO}$ decreases from
684 \$0.7505/m^3 to \$0.6995/m^3 when freshwater capacity increases from 10,000 m^3/day to
685 40,000 m^3/day. For a constant freshwater capacity of 20,000 m^3/day, when the cooling
686 capacity increases from 5,000 kW to 20,000 kW, the $LCOW_{RO}$ increases slightly from
687 \$0.7209/m^3 to \$0.7237/m^3. This slight increase in the $LCOW_{RO}$ is due to a small increase in
688 the $LCOE$. As expected, TAC_{total} increases with an increase in the demands. A more
689 noticeable increase is observed when freshwater demands increase.
690
691 **Table 13-** Effect of change in the cooling and freshwater demands on the thermodynamic and
692 economic performances of configuration 1.

Demands	η_{GTCC}	$LCOE$	$LCOW_{RO}$

		$(\frac{\$}{kWh})$	$(\frac{\$}{m^3})$
5,000 kW/20,000 m^3/day	0.4581	0.0645	0.7209
10,000 kW/20,000 m^3/day	0.4535	0.0648	0.7219
15,000 kW/20,000 m^3/day	0.4491	0.0651	0.7228
20,000 kW/20,000 m^3/day	0.4447	0.0654	0.7237
10,000 kW/10,000 m^3/day	0.4589	0.0641	0.7505
10,000 kW/20,000 m^3/day	0.4535	0.0648	0.7219
10,000 kW/30,000 m^3/day	0.4483	0.0655	0.7080
10,000 kW/40,000 m^3/day	0.4431	0.0662	0.6995

5.1. Parametric studies

This section presents the parametric study results to investigate the influences of some of the most important design and operating parameters on the performance of the hybrid configuration 1, as most economically viable hybrid trigeneration configuration.

5.1.1. Effect of wet bulb and ambient temperatures

Fig. 4 shows the impact of wet bulb temperature (T_{wb}) on the thermodynamic efficiency of the gas turbine combined cycle and Rankine cycle. As noted in Section 3, it was assumed that ambient temperature (T_{amb}), or dry bulb temperature, is 10 K higher than T_{wb}. Thus, in the analysis, both T_{amb} and T_{wb} vary with a fixed 10 K difference. This 10 K temperature difference may not be the case for many locations; however, the main objective is to examine the impact of variation of both T_{amb} and T_{wb} on the thermodynamic efficiency. An increase in the T_{wb} causes an increase in the condensation stage temperature of the Rankine cycle and negatively impacts the performance of the wet cooling system. Thus, when T_{wb} increases from 293 K to 303 K, η_{Rank} reduces from 0.334 to 0.3203. A change in the T_{amb} slightly impacts the performance of the gas turbine cycle. An increase in the T_{amb} from 303 K to 313 K and an increase in T_{wb} from 293 K to 303 K, leads to a reduction in the η_{GTCC} from 0.4579 to 0.4486. The analysis of the impact of T_{wb} and T_{amb} is very useful to determine how the performance of trigeneration system changes if the system is built in different locations with different design ambient temperatures.

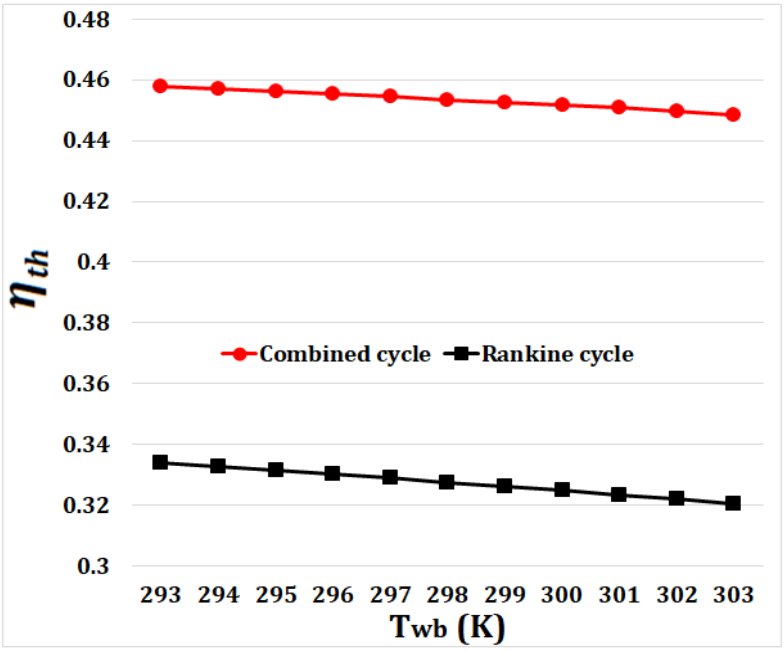

Fig. 4. Effect of T_{wb} and T_{amb} on the η_{th} of combined cycle and Rankine cycle.

Examining the effects of T_{wb} and T_{amb} on the TAC_{total} and TAC_{ABC} showed that with an increase in T_{wb} and T_{amb}, TAC_{total} and TAC_{ABC} increase from \$49,030,000/year to \$49,904,000/year and from \$666,000/year to \$817,000/year, respectively. The main reason for the increase in the TAC_{total} is due to an increase in the AOC of the combined cycle as the rate of fuel consumption goes up with a reduction in η_{th}. At higher T_{wb}, the steam requirements of the ABC cycle increases leading to an increase in the size of different components to generate the same cooling capacity. This causes an increase in the capital cost and ACC of the ABC cycle. Moreover, an increase in the LCOE causes a small increase in the AOC of the ABC cycle.

Fig. 5. illustrates the influences of T_{wb} and T_{amb} on LCOE and LCOC. It is observed that with an increase in T_{wb} and T_{amb}, the LCOE increases from \$0.0643/kWh to \$0.0653/kWh mainly due to an increase in the AOC of the combined cycle. LCOC experiences a relatively high increase from \$0.0468/ton-hr to \$0.0575/ton-hr due to an increase in both ACC and AOC of the ABC cycle.

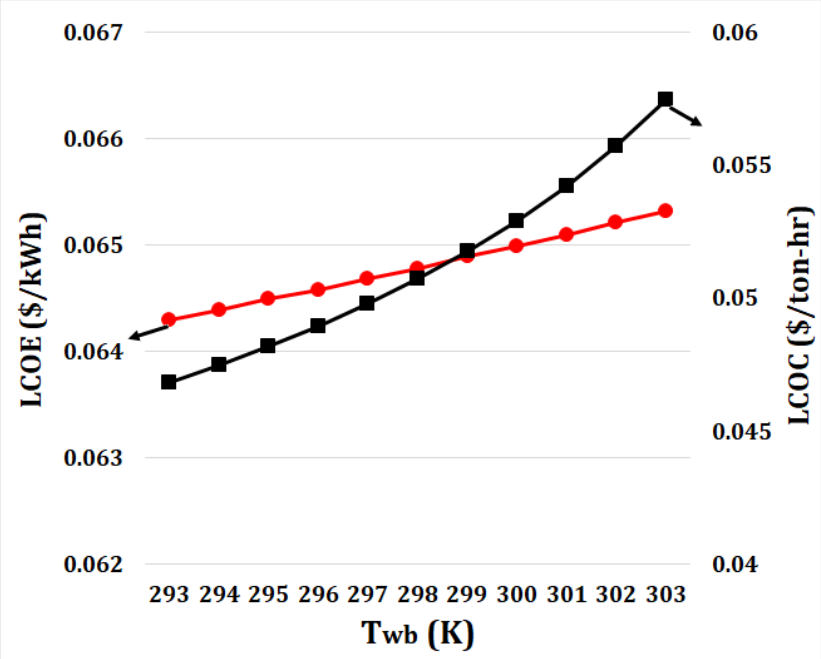

Fig. 5. Effect of T_{wb} and T_{amb} on the LCOE and LCOC.

5.1.2. Effect of salinity and temperature of feed seawater

Fig. 6 shows that a change in the X_F has a large impact on the $\dot{W}_{pump,RO}$ and LCOW of the RO unit. When the salinity of feed seawater increases, the performance of the RO unit decreases significantly. This causes an increase in the total amount of pumping power required to generate the same amount of freshwater using the RO unit. Analyzing the impact of X_F is important because the salinity of seawater varies from one location to another. Thus, the performance of an RO unit may vary significantly when it is built in different locations. The salinity of seawater has one of its highest value in the Persian Gulf which is close to 46,000 ppm while it has much lower values in Mediterranean Sea (38,000 ppm) and north Australia (35,000 ppm). According to Fig. 6, with an increase in the X_F from 30,000 ppm to 50,000 ppm, $\dot{W}_{pump,RO}$ increases by almost 64% from 1,919 kW to 3,156 kW. The LCOW increases from \$0.659/m^3 to \$0.805/m^3 which means over a 22% increase. A comparison between building the plant in a location in the Persian Gulf and a location in north Australia indicates around a 31% increase in the pumping power requirement.

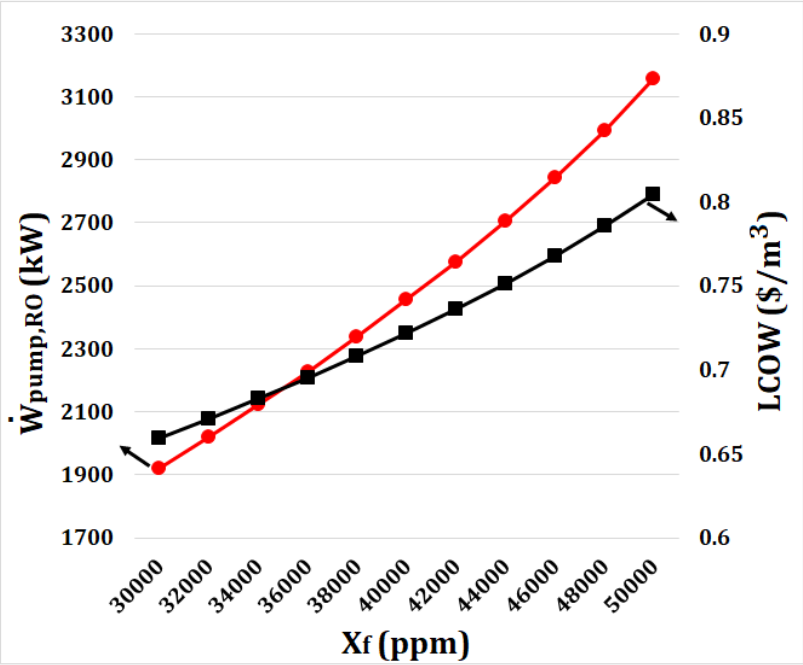

Fig. 6. Effect of X_F on the $\dot{W}_{pump,RO}$ and LCOW.

Another examination showed that an increase in the X_F causes an increase in the TAC_{total} and TAC_{RO}. An increase in the X_F leads to an increase in the AOC_{GTCC} due to increasing the gross power of the combined cycle. While the impact of X_F on the ACC of the combined cycle is very small. Also, when X_F increases, both AOC and ACC (TAC_{RO}) of the RO system increases. The increase in the TAC_{RO} and AOC_{GTCC} causes an increase in the TAC_{total}. With an increase of X_F from 30,000 to 50,000 ppm, TAC_{total} increases from \$48,8510,000/year to \$50,183,000/year and TAC_{RO} increases from \$3,848,000/year to \$4,699,000/year, respectively.

Fig. 7 shows the effect of T_F on the $\dot{W}_{pump,RO}$ and LCOW. As shown in Fig. 7, an increase in the feed seawater temperature (T_F) causes a reduction in the $\dot{W}_{pump,RO}$ and LCOW of the RO unit. This demonstrates that if the input feed seawater is preheated or when the plant is built in locations with higher T_F, better performance and lower LCOW is obtained for the plant. The average temperatures of seawater for the Mediterranean Sea, north Australia (Indian Ocean) and the Persian Gulf are around 26 °C, 31 °C, and 36 °C, respectively [44]. Thus, the RO plants built in the Persian Gulf have better performance and lower LCOW. However, the warmer climates of the locations in the Persian Gulf negatively influence the performance of the gas turbine combined cycle and the absorption chiller.

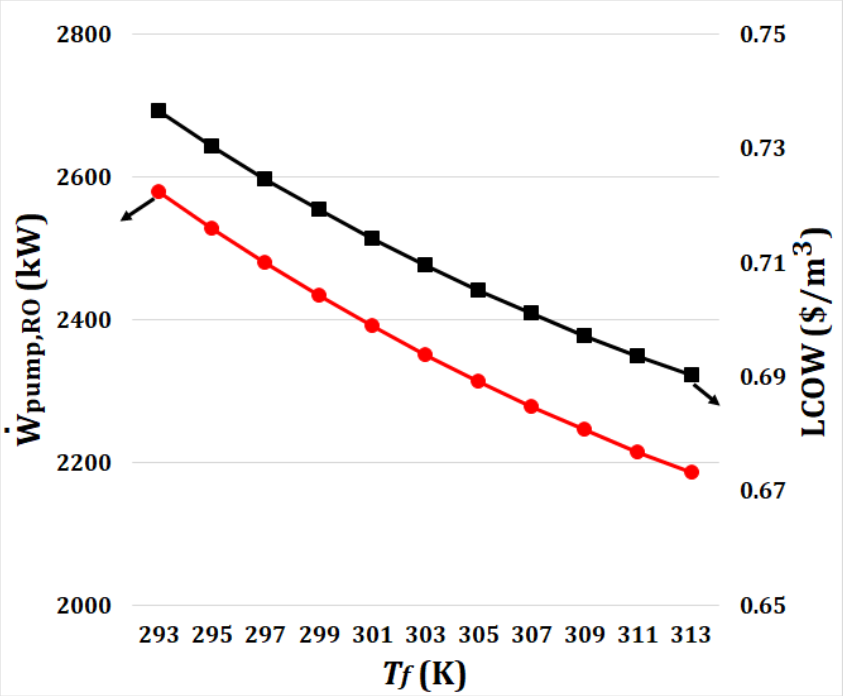

Fig. 7. Effect of T_F on the $\dot{W}_{pump,RO}$ and LCOW.

5.1.3. Effect of compressor pressure ratio

Fig. 8 shows the influence of a variation in the compressor pressure ratio (PR) on the η_{th} of the combined cycle and Brayton cycle. An increase in PR from 8 to 20 leads to a significant increase in the η_{th} of the Brayton cycle from 0.293 to 0.352. However, an increase in PR decreases the steam generated in the HRSG which consequently reduces the net power production by the steam Ranking cycle and η_{th} of the Rankine cycle. When PR increases from 8 to 20, η_{th} of the Rankine cycle slightly reduces from 0.331 to 0.324. Due to this increase in η_{th} of the Brayton cycle and a decrease in η_{th} of the Rankine cycle, η_{th} of the Brayton cycle initially increases from 0.442 at PR of 8 to 0.456 at PR of 15 which is its maximum value. Further increase after PR of 15 causes a decrease in η_{th} of the Brayton cycle which reaches 0.452 at PR of 20.

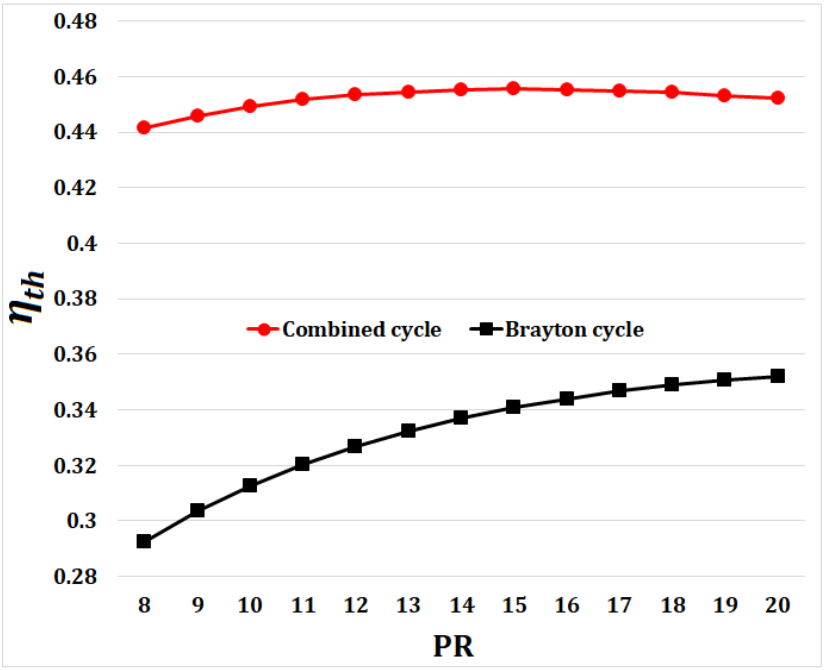

Fig. 8. Effect of PR on the η_{th} of the combined cycle and Brayton cycle.

Conducting more analysis revealed that ACC_{GTCC} and AOC_{GTCC} have different trends of variation with an increase in PR. ACC_{GTCC} has an almost constant increasing pattern when PR increases. While AOC_{GTCC} has an almost opposite trend of variation as that η_{th} of the combined cycle such that it initially decreases because of an increase in η_{th} and then increases with a further increase in PR. Overall, when PR increases, TAC_{GTCC} initially decreases from \$45,167,000/year to \$44,493,000/year at an optimum PR of 12.1 and then increases with more increase in PR. As the size of DEABC and RO systems are constant, PR does not have any impact on ACC_{ABC} and ACC_{RO}. While the effect of PR on AOC_{ABC} is negligible, due to the minimum electricity requirement of the DEABC cycle, its impact on AOC_{RO} is similar to that of TAC_{GTCC}.

Fig. 9 shows how a change in PR causes a variation in the LCOE and LCOW. As expected, the optimum values of LCOE and LCOW are both obtained at a PR of around 12. When PR increases from 8 to 12, LCOE and LCOW vary from \$0.0658/kWh to \$0.0648/kWh and from \$0.725/m^3 to \$0.722/m^3, respectively. After PR of 12, LCOE and LCOW constantly increase until they reach the values of \$0.0669/kWh and \$0.728/m^3 at PR of 20.

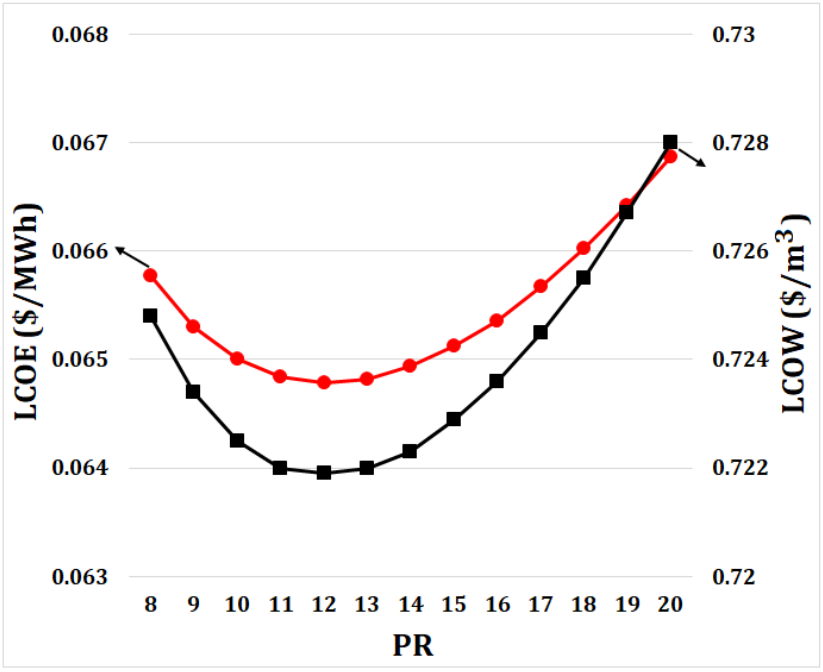

Fig. 9. Effect of PR on the LCOE and LCOW.

5.1.4. Effect of turbine inlet temperature of the gas turbine cycle

The effect of turbine inlet temperature of the gas turbine cycle, or Brayton cycle, ($TIT_{Brayton}$) on the η_{th} of the combined cycle and Brayton cycle is shown in Fig. 10. It is observed that an increase in the $TIT_{Brayton}$ from 1,373 K to 1,573 K leads to a noticeable increase in the η_{th} of the combined cycle from 0.427 to 0.466. An increase in the $TIT_{Brayton}$ from 1,373 K to 1,573 K causes an increase in the η_{th} of the Brayton cycle from 0.317 to 0.332. With an increase in the $TIT_{Brayton}$, the exhaust temperature from the gas turbine increases. Thus, η_{th} of the Rankine cycle increases slightly from 0.326 to 0.328 when $TIT_{Brayton}$ increases from 1,373 K to 1,573 K. The combination of an increase in the η_{th} of the Brayton cycle and Rankine cycle causes an increase in the η_{th} of the combined cycle.

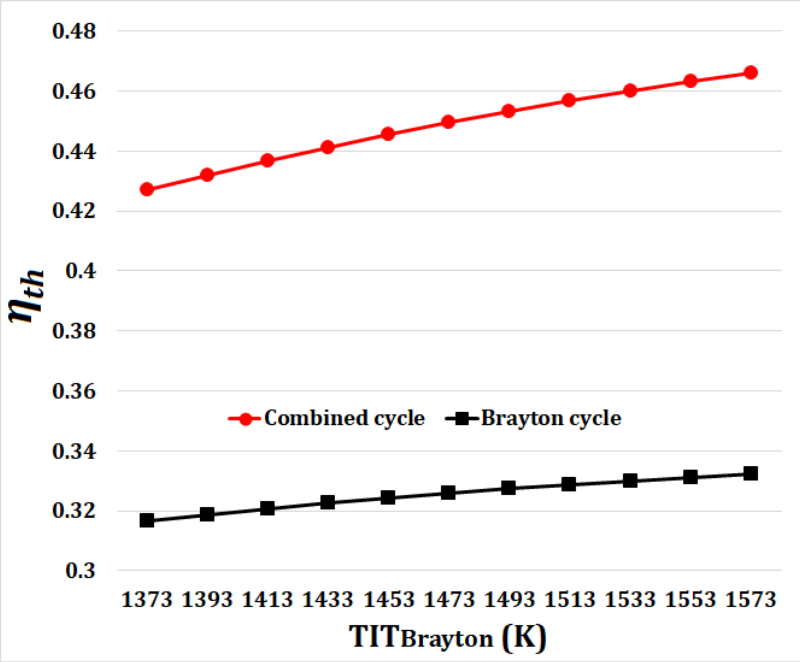

Fig. 10. Effect of $TIT_{Brayton}$ on the η_{th} of the combined cycle and Brayton cycle.

Another analysis was carried out to investigate the impact of $TIT_{Brayton}$ on TAC_{total} and TAC_{RO}. As shown in Fig. 10, an increase in the $TIT_{Brayton}$ improves the η_{th} of the Brayton cycle leading to a reduction in fuel consumption and AOC. However, with an increase in the $TIT_{Brayton}$, the ACC of the gas turbine cycle decreases until an optimal $TIT_{Brayton}$ (1,495 K) and then it increases with further increase in the $TIT_{Brayton}$. While AOC_{GTCC} has a constant decreasing pattern, the increase in the ACC_{GTCC} at higher $TIT_{Brayton}$ (after 1,495 K) is higher than the decrease in the AOC_{GTCC} leading to an increase in the TAC_{GTCC}. While an increase in the $TIT_{Brayton}$ has almost no impact on the TAC_{ABC}, it causes an increase in the AOC_{RO} due to an increase in the LCOE. Thus, as observed, TAC_{RO} has the same decreasing and increasing pattern as that of TAC_{total}.

Fig. 11 illustrates the effect of $TIT_{Brayton}$ on the LCOE and LCOW. As shown, both $LCOE$ and $LCOW$ have a decreasing and increasing pattern (similar to TAC_{total} and TAC_{RO}) when $TIT_{Brayton}$ increases. With an increase in $TIT_{Brayton}$ from 1373K to 1495 K (the optimum value presented in Table 6), the LCOE and LCOW reduce from \$0.0673/kWh to \$0.0648/kWh, and from \$0.7294/m^3 to \$0.7219/m^3, respectively. From 1495 K to 1573 K, the LCOE and LCOW increase substantially to \$0.0713/kWh and \$0.7411/m^3, respectively.

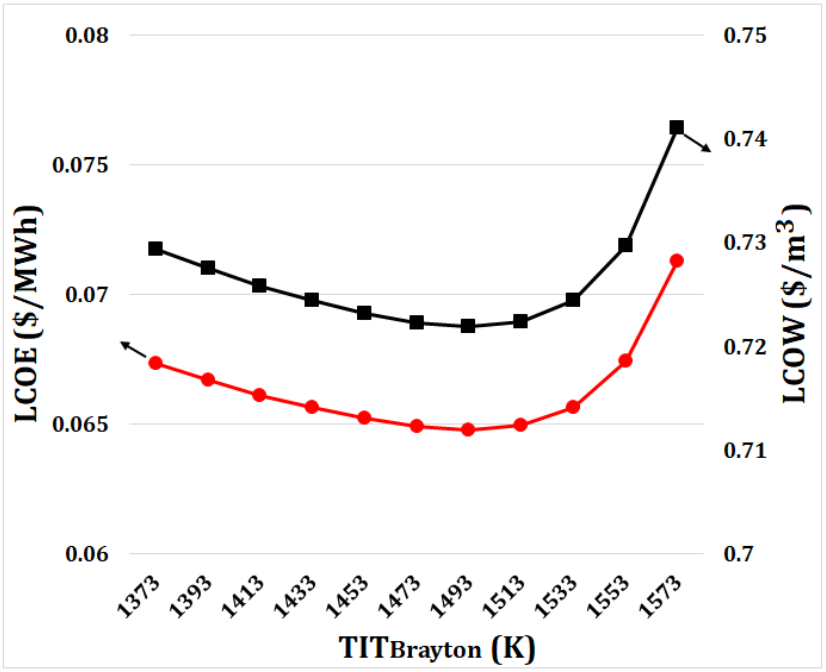

Fig. 11. Effect of $TIT_{Brayton}$ on the LCOE and LCOW.

5.1.5. Effect of gas turbine combined cycle size

Fig. 12 illustrates the effects of change in the size of the gas turbine combined cycle ($\dot{W}_{net,GTCC}$) on the TAC_{total} and TAC_{RO}. The influence of $\dot{W}_{net,GTCC}$ on the LCOE and LCOW is shown in Fig. 13. Note that for these analyses, the cooling and freshwater production capacities remain constant at 10,000 kW and 20,000 m^3/day. With an increase in $\dot{W}_{net,GTCC}$, both ACC_{GTCC} and AOC_{GTCC} increase, due to the growth in the size of the plant. It is observed that TAC_{RO} experiences a small reduction due to a decrease in the LCOE, as shown in Fig. 12. Note that TAC_{ABC} has almost no change when $\dot{W}_{net,GTCC}$ increases. The combination of an increase in the ACC_{GTCC} and AOC_{GTCC} causes a significant increase in the TAC_{total} from \$28,696,000/year to \$69,066,000/year. As mentioned and shown in Fig. 13, with an increase in the $\dot{W}_{net,GTCC}$ from 50,000 kW to 150,000 kW, the LCOE decreases from \$0.070/kWh to \$0.0626/kWh. The LCOW decreases from \$0.7372/m^3 to \$0.7156/m^3 due to a reduction in the AOC_{RO}, as a result of a reduction in the LCOE.

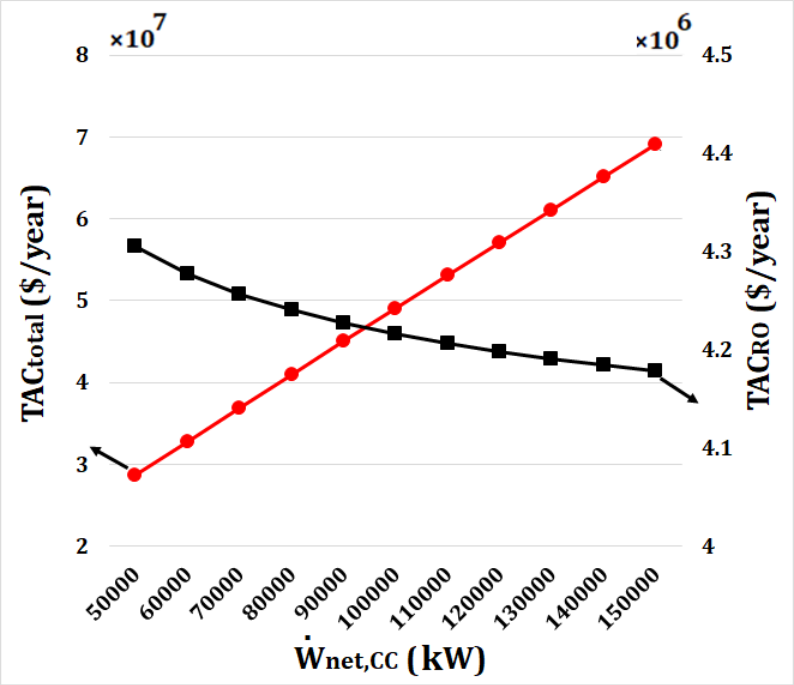

Fig. 12. Effect of $\dot{W}_{net,GTCC}$ on the TAC_{total} and TAC_{RO}.

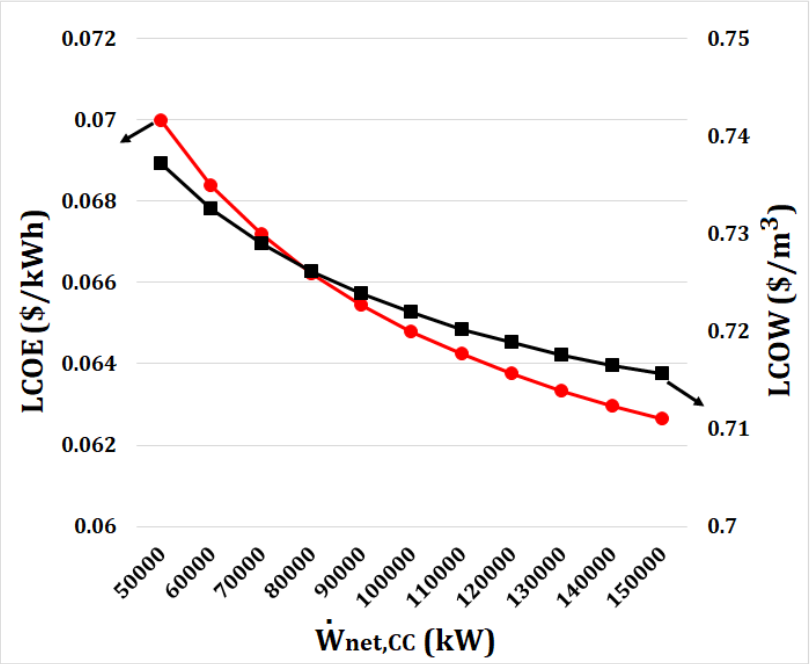

Fig. 13. Effect of $\dot{W}_{net,GTCC}$ on the LCOE and LCOW.

6. Conclusions

This study evaluated the feasibility of hybrid trigeneration systems based on a gas turbine combined cycle with steam for generating electricity, freshwater, and cooling.

The thermodynamic results showed that the highest thermodynamic efficiency of the combined cycle was found for configuration 2 (0.4552) and the lowest value (0.4457) was

found for configuration 5 with a 4-effect MED. The results for configurations 5 and 6 showed that an increase in the number of effects led to an increase in the productivity of the MED plant and consequently a reduction in the RO's share of water generation. Due to the higher specific power consumption of the RO than the MED, increasing the number effects caused a reduction in the gross power that should be generated to produce the same amount of freshwater, and as a result, an increase in thermodynamic efficiency of the combined cycle.

The economic results demonstrated that configuration 1, which integrated an RO unit and an DEABC to the combined cycle, was the most economical configuration. Configuration 1 had 5.98% less TAC_{total} than configuration 5 with an 8-effect MED unit, as the least economical hybrid configuration. Implementation of RO was found to be more economical than a hybrid MED-RO system. Also, using DEABC which operated using the extracted steam from the steam bottoming cycle was found to be more economical than both HEABC and VCC. Although the ACC of the VCC was found to be significantly lower than that of the DEABC, its AOC was obtained almost nine times higher. For configuration 1, the LCOE, LCOW, LCOC were \$64.78/MWh, \$0.7219/m^3 and \$0.0402/ton-hr, respectively, whose LCOE and LCOC were not the lowest values among different configurations.

In summary, the findings of this study provided some useful guides on the development of hybrid trigeneration systems based on a gas turbine combined power plant, as the most growing and clean fossil fuel-based power plant. Such hybrid trigeneration systems are beneficial due to their ability to improve energy utilization efficiency and reduce fuel consumption leading to cleaner production of the products. Their development will also lead to decreasing both capital and operating costs and reducing CO_2 emissions. Future studies should be investigated to evaluate the dynamic performance of the hybrid trigeneration systems. Also, a solar tower system that uses pressurized air receiver can be integrated into the gas turbine combined cycle to reduce the fuel consumption and make the trigeneration systems even more sustainable and cleaner.

Acknowledgement

The authors are grateful for the funding sources provided by the U.S. Department of Energy's office of Energy Efficiency and Renewable Energy under Grant Number DE-EE0007712.

References

[1] Gianluca Valenti, Alessandro Valenti, Simone Staboli. Proposal of a thermally-driven air compressor for waste heat recovery. Energy Conversion and Management 196 (2019) 1113–1125.

[2] Giovanni Manente, Francesca Maria Fortuna. Supercritical CO2 power cycles for waste heat recovery: A systematic comparison between traditional and novel layouts with dual expansion. Energy Conversion and Management 197 (2019) 111777.

[3] J. Deng, R. Wang and G. Han, "A review of thermally activated cooling technologies for combined cooling, heating and power systems," Progress in Energy and Combustion Science, vol. 37, no. 2, pp. 172-203, 2011.

[4] Arash Mollahosseini, Amira Abdelrasoul, Sina Sheibany, Maryam Amini, Saeed Khoshhal Salestan. Renewable energy-driven desalination opportunities – A case study. Journal of Environmental Management 239 (2019) 187–197

[5] G. Beretta, P. Iora and A. Ghoniem, "Allocating resources and products in multi-hybrid multi-cogeneration: What fractions of heat and power are renewable in hybrid fossil-solar CHP?," Energy, vol. 78, pp. 587-603, 2014.
[6] Pouria Ahmadi. Modeling, Analysis and Optimization of Integrated Energy Systems for Multigeneration Purposes. University of Ontario Institute of Technology, PhD dissertation. 2013.
[7] Pouria Ahmadi, Ibrahim Dincer, Marc A. Rosen. Performance assessment and optimization of a novel integrated multigeneration system for residential buildings. Energy and Buildings 67 (2013) 568–578.
[8] P. Ahmadi, I. Dincer and M. Rosen, "Multi-objective optimization of a novel solar-based multigeneration energy system," Solar Energy, vol. 108, pp. 576-591, 2014.
[9] S. Karellas and K. Braimakis, "Energy–exergy analysis and economic investigation of a cogeneration and trigeneration ORC–VCC hybrid system utilizing biomass fuel and solar power," Energy conversion and management, vol. 107, pp. 103-113, 2016.
[10] B. Patel, N. Desai, S. Kachhwaha, V. Jain and N. Hadia, "Thermo-economic analysis of a novel organic Rankine cycle integrated cascaded vapor compression–absorption system," Journal of cleaner production, pp. 26-40, 2017.
[11] R. El-Emam and I. Dincer, "Development and assessment of a novel solar heliostat-based multigeneration system," International Journal of Hydrogen Energy, vol. 43, no. 5, pp. 2610-2620, 2018.
[12] Simin Anvari, Hadi Taghavifar, Alireza Parvishi. Thermo-economical consideration of Regenerative organic Rankine cycle coupling with the absorption chiller systems incorporated in the trigeneration system. Energy Conversion and Management 148 (2017) 317–329.
[13] Pooria Behnam, Alireza Arefi, Mohammad Behshad Shafii. Exergetic and thermoeconomic analysis of a trigeneration system producing electricity, hot water, and fresh water driven by low-temperature geothermal sources. Energy Conversion and Management 157 (2018) 266–276.
[14] Shoaib Khanmohammadi, Kazem Atashkari. Modeling and multi-objective optimization of a novel biomass feed polygeneration system integrated with multi effect desalination unit. Thermal Science and Engineering Progress 8 (2018) 269–283.
[15] Saeed Ghavami Gargari, Mostafa Rahimi, Hadi Ghaebi. Energy, exergy, economic and environmental analysis and optimization of a novel biogas-based multigeneration system based on Gas Turbine-Modular Helium Reactor cycle. Energy Conversion and Management 185 (2019) 816–835.
[16] Mohammad Zoghi, Hamed Habibi, Ata Chitsaz, Mojtaba Ayazpour, Parisa Mojaver. Thermo-economic assessment of a novel trigeneration system based on coupling of organic Rankine cycle and absorption-compression cooling and power system for waste heat recovery. Energy Conversion and Management 196 (2019) 567–580.
[17] M. Bottarelli, M. Cannistraro, E. Mainardi, Testing a dual-source heat pump, Mathematical Modelling of Engineering Problems Vol. 5, No. 3, Sept. 2018, pp. 205-210, https://doi.org/10.18280/mmep.050311
[18] Aida Farsi, Ibrahim Dincer. Development and evaluation of an integrated MED/membrane desalination system. Desalination 463 (2019) 55–68.
[19] Farid Safari, Ibrahim Dincer. Development and analysis of a novel biomass-based integrated system for multigeneration with hydrogen production. International journal of hydrogen energy 44 (2019) 3511-3526.
[20] Anoop Kumar Shukla, Onkar Singh. Thermodynamic investigation of parameters affecting the execution of steam injected cooled gas turbine based combined cycle power plant with vapor absorption inlet air cooling. Applied Thermal Engineering 122 (2017) 380–388.
[21] Alok K. Mohapatra, Sanjay. Exergetic evaluation of gas-turbine based combined cycle system with vapor absorption inlet cooling. Applied Thermal Engineering 136 (2018) 431–443.
[22] G. Cannistraro, M. Cannistraro, A. Galvagno, G. Trovato:" Technical and economic evaluations about the integration of co-Trigeneration systems in the dairy industry", IJH&T, vol. 34, S.I.2, Oct. 2016, pp 332, 336. DOI: 10.18280/ijht.34S220

955 [23] A. Cannistraro, G. Cannistraro, M. Cannistraro, A. Galvagno, G. Trovato: "Evaluation on the convenience of a
956 citizen service district hating for residential use. A new scenario introduced by high efficiency energy
957 systems". *IJH&T*, Vol.33, N°4, 2015.
958 DOI:10.18280 http://www.iieta.org/sites/default/files/Journals/HTECH/ 33.04.21.pdf
959 [24] Mayank Maheshwari, Onkar Singh. Comparative evaluation of different combined cycle configurations
960 having simple gas turbine, steam turbine and ammonia water turbine. Energy 168 (2019) 1217-1236.
961 [25] Ali Amini, Nima Mirkhani, Pedram Pakjesm Pourfard, Mehdi Ashjaee, Mohammad Amin Khodkar Thermo-
962 economic optimization of low-grade waste heat recovery in Yazd combined-cycle power plant (Iran) by a CO_2
963 transcritical Rankine cycle. Energy 86 (2015) 74-84.
964 [26] Jatin Sachdeva, Onkar Singh. Thermodynamic analysis of solar powered triple combined Brayton, Rankine
965 and organic Rankine cycle for carbon free power. Renewable Energy 139 (2019) 765-780.
966 [27] D. Kroger, Air-Cooled Heat Exchangers and Cooling Towers: Thermal-Flow Performance Evaluation and
967 Design, Vol. 1. 2004 by PennWell Corporation.
968 [28] D. Kroger, Air-Cooled Heat Exchangers and Cooling Towers: Thermal-Flow Performance Evaluation and
969 Design, Vol. 2. 2004 by PennWell Corporation.
970 [29] El-Dessouky HT, Ettouney HM. Fundamentals of salt water desalination. Elsevier; 2002.
971 [30] Herold, K.E., Radermacher, R., Klein, S.A., 2016. Absorption Chillers and Heat Pumps. 786 611 CRC Press,
972 Boca Raton, Florida.
973 [31] M.H. Khoshgoftar Manesh, H. Ghalami, M. Amidpour, M.H. Hamedi. Optimal coupling of site utility steam
974 network with MED-RO desalination through total site analysis and exergoeconomic optimization. Desalination
975 316 (2013) 42–52.
976 [32] Engineering equation solver (EES), 2019. Commercial V 10.620, #5515. < www.fchart.com/ees >.
977 [33] Walraven Daniel, Laenen Ben, D'haeseleer William. Economic system optimization of air-cooled organic
978 Rankine cycles powered by low-temperature geothermal heat sources. Energy 2015;80:104–13.
979 [34] M. H. Sharqawy, J. H. Lienhard, S. M. Zubair. The thermophysical properties of seawater: A review of
980 existing correlations and data. Desalination and Water Treatment, 16 (April 2010) 354–380.
981 [35] Ibrahim S. Al-Mutaz, Irfan Wazeer Comparative performance evaluation of conventional multi-effect
982 evaporation desalination processes. Applied Thermal Engineering 73 (2014) 1194-1203.
983 [36] A.S. Nafey, M.A. Sharaf Combined solar organic Rankine cycle with reverse osmosis desalination process:
984 Energy, exergy, and cost evaluations. Renewable Energy 35 (2010) 2571-2580.
985 [37] Mohammadreza Khanarmuei, Hossein Ahmadisedigh, Iman Ebrahimi, Louis Gosselin, Hamid Mokhtari.
986 Comparative design of plug and recirculation RO systems; thermoeconomic: Case study. Energy 121 (2017)
987 205-219.
988 [38] Hamid Mokhtari, Mehdi Sepahvand, Ahmad fasihfar. Thermoeconomic and exergy analysis in using
989 hybrid systems (GT+MED+ RO) for desalination of brackish water in Persian Gulf. Desalination 399 (2016) 1–
990 15.
991 [39] Bilal Ahmed Qureshi, Syed M. Zubair Exergetic. analysis of a brackish water reverse osmosis desalination
992 unit with various energy recovery systems. Energy 93 (2015) 256-265.
993 [40] Bilal Ahmed Qureshi, Syed M. Zubair. Energy-exergy analysis of seawater reverse osmosis plants.
994 Desalination 385 (2016) 138–147.
995 [41] Mohammad Saghafifar. Thermo-economic optimization of hybrid combined power cycles using heliostat
996 solar field. American University of Sharjah; 2016. Master of Science thesis.
997 [42] James D. Spelling. Hybrid Solar Gas-Turbine Power Plants: A Thermoeconomic
998 Analysis. KTH Royal Institute of Technology, PhD thesis, 2013.

[43] Kasra Mohammadi, Jon G. McGowan. An efficient integrated trigeneration system for the production of dual temperature cooling and fresh water: Thermoeconomic analysis and optimization. Applied Thermal Engineering, 145, (2018), 652-666.
[44] M. Mosera, F. Trieb, T. Fichter, J. Kern, H. Maier, P. Schicktanz. Techno-economic analysis of enhanced dry cooling for CSP. Energy Procedia 49 (2014) 1177 – 1186.
[45] Smith R. Chemical process design and integration. John Wiley & Sons Ltd; 2005.
[46] World Energy, 2015. Absorption Chiller Absorption Chiller & Heater Absorption Heat Pump. Available at: http://www.worldenergyeurope.eu/down/wecat.pdf.
[47] Ighball Baniasad Askari, Mehran Ameri, Francesco Calise. Energy, exergy and exergo-economic analysis of different water desalination technologies powered by Linear Fresnel solar field. Desalination 425 (2018) 37–67.